

# Short-range correlation physics at low renormalization group (RG) resolution

**Anthony Tropiano<sup>1</sup>, Scott Bogner<sup>2</sup>, Dick Furnstahl<sup>1</sup>**

<sup>1</sup>Ohio State University, <sup>2</sup>Michigan State University

TRIUMF seminar

December 16, 2021

*ajt, S.K. Bogner, and R.J. Furnstahl, arXiv:2105.13936*

*Phys. Rev. C **104**, 034311 (2021)*

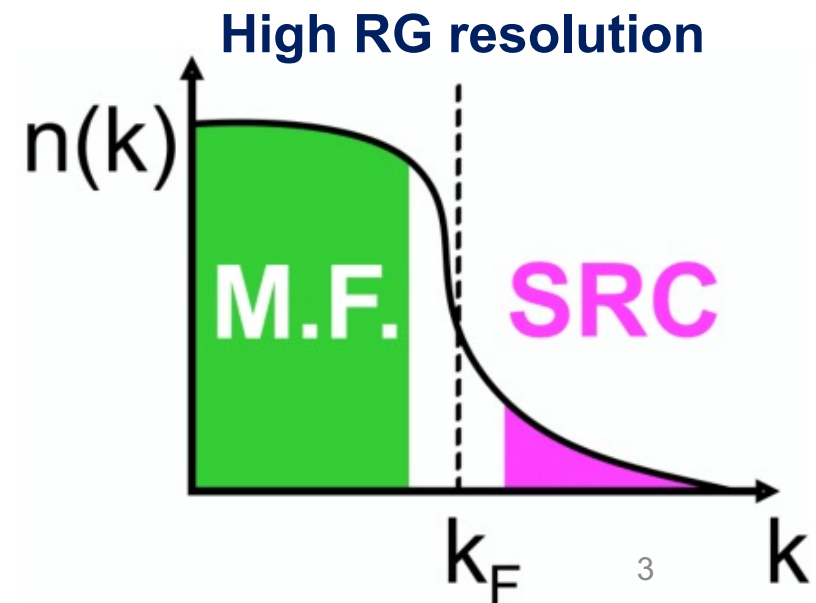


# Short-range correlations

- Recent experiments have been able to isolate processes where short-range correlation (SRC) physics is dominant and well accounted for by SRC phenomenology
- How are short-range correlations defined?
  - Depends on the resolution scale!
  - Renormalization group (RG) resolution scale is set by  $\Lambda$  in the Hamiltonian  $H(\Lambda)$
  - $\Lambda \sim$  max momenta in low-energy wave functions

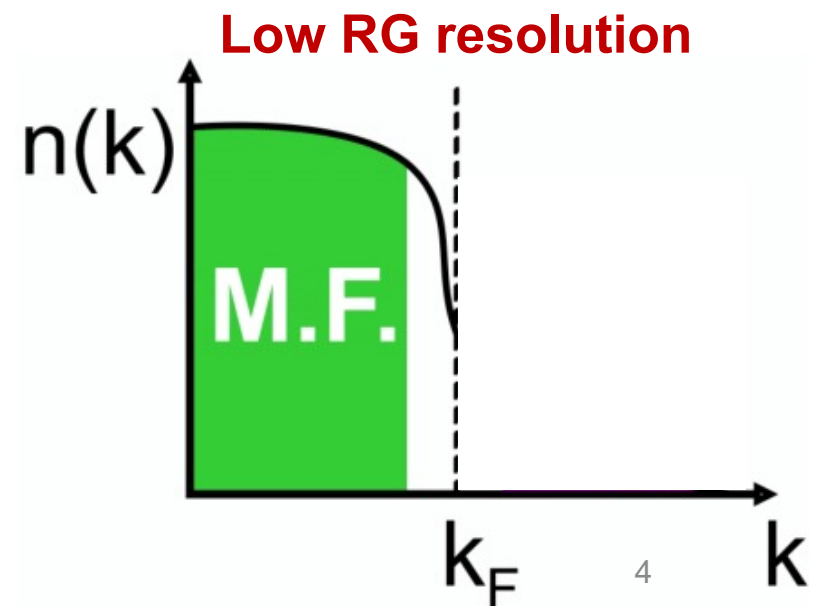
# High and low RG resolution

- SRC physics at high RG resolution
  - SRC pairs are components in the nuclear wave function with relative momenta well above the Fermi momentum  $k_F$  and CM momentum  $< k_F$



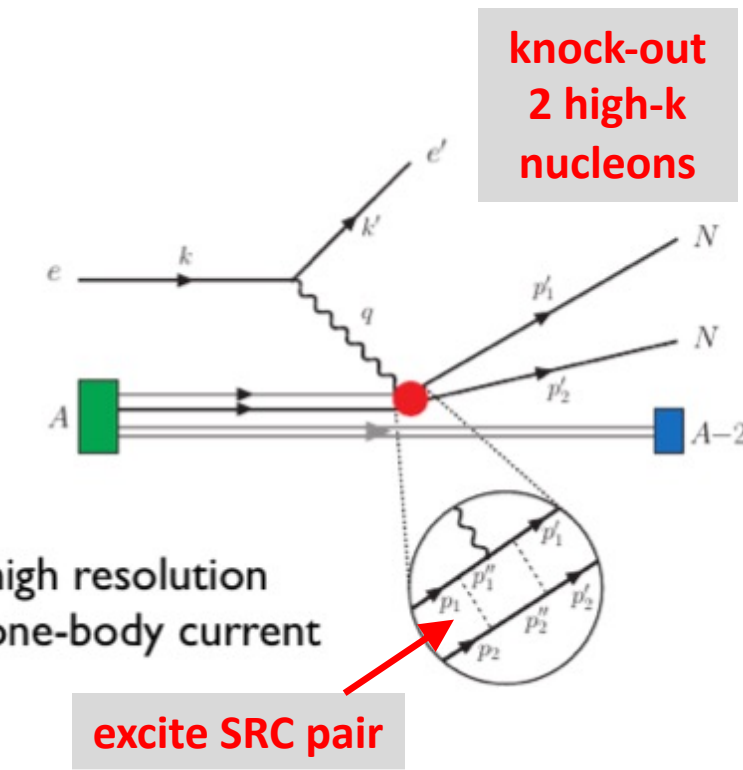
# High and low RG resolution

- SRC physics at high RG resolution
  - SRC pairs are components in the nuclear wave function with relative momenta well above the Fermi momentum  $k_F$  and CM momentum  $< k_F$
- SRC physics at low RG resolution
  - The SRC *physics* is shifted into the reaction operators from the nuclear wave function (which becomes soft)



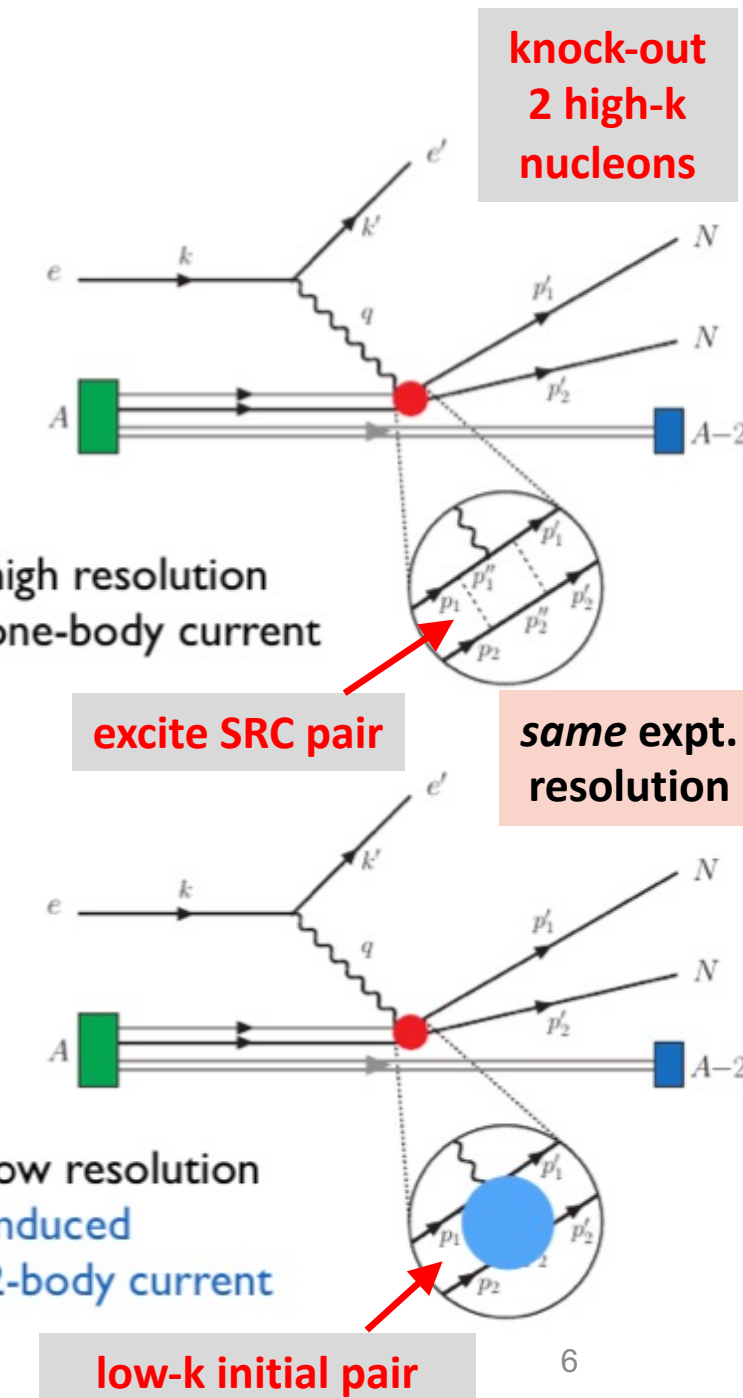
# High and low RG resolution

- High RG resolution: One-body current operators with correlated wave functions



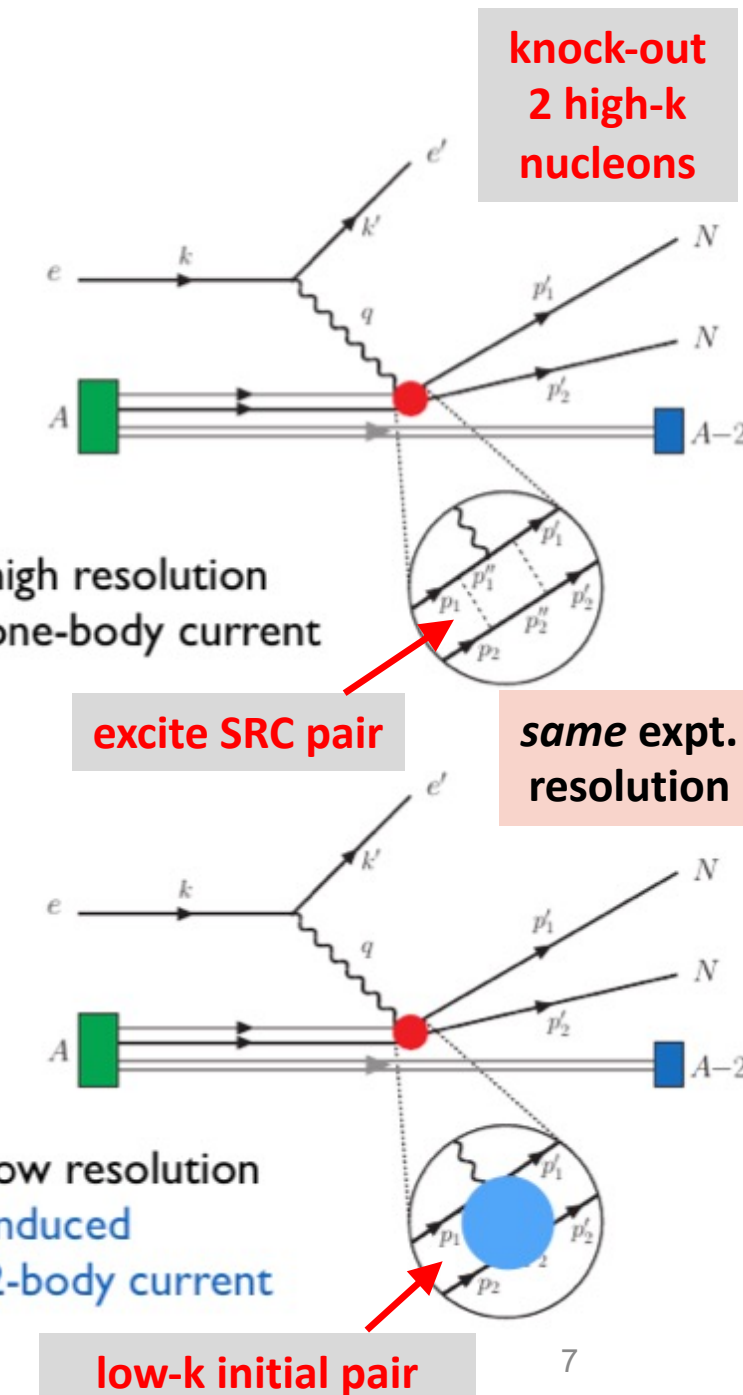
# High and low RG resolution

- High RG resolution: One-body current operators with correlated wave functions
- Low RG resolution: Two-body current operators with uncorrelated wave functions
  - Operators do NOT become hard, which simplifies calculations!



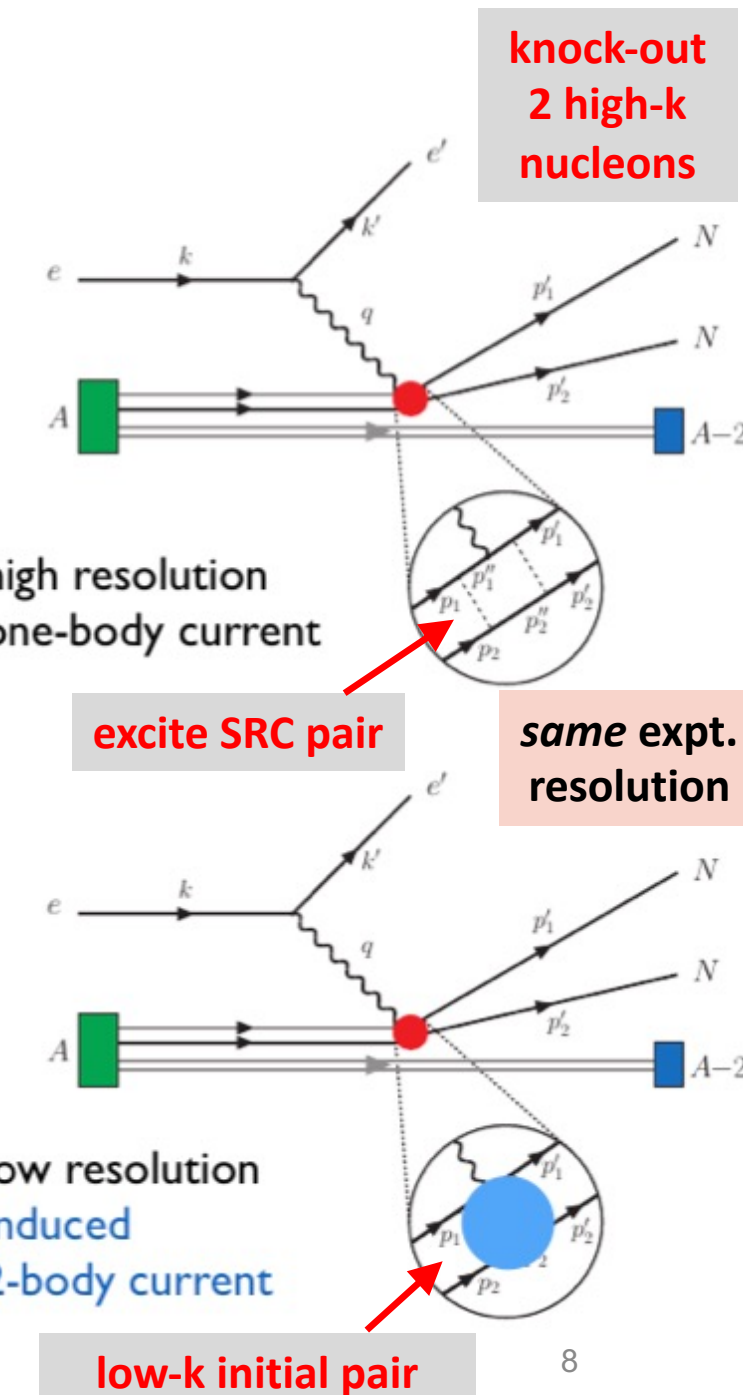
# High and low RG resolution

- High RG resolution: One-body current operators with correlated wave functions
- Low RG resolution: Two-body current operators with uncorrelated wave functions
  - Operators do NOT become hard, which simplifies calculations!
- Experimental resolution (set by momentum of probe) is the same in both pictures
- Same observables but different physical interpretation!



# High and low RG resolution

- High RG resolution: One-body current operators with correlated wave functions
- Low RG resolution: Two-body current operators with uncorrelated wave functions
  - Operators do NOT become hard, which simplifies calculations!
- Experimental resolution (set by momentum of probe) is the same in both pictures
- Same observables but different physical interpretation!
- This talk:
  - How can SRC calculations be carried out at low RG resolution?
  - What can we describe with simple approximations?
  - Connections to existing SRC phenomenology (e.g., GCF/LCA)



# Similarity renormalization group

- Evolve to low RG resolution using the SRG

$$O(s) = U(s)O(0)U^\dagger(s)$$

where  $s = 0 \rightarrow \infty$  and  $U(s)$  is unitary

- SRG transformations decouple high- and low-momenta in the Hamiltonian

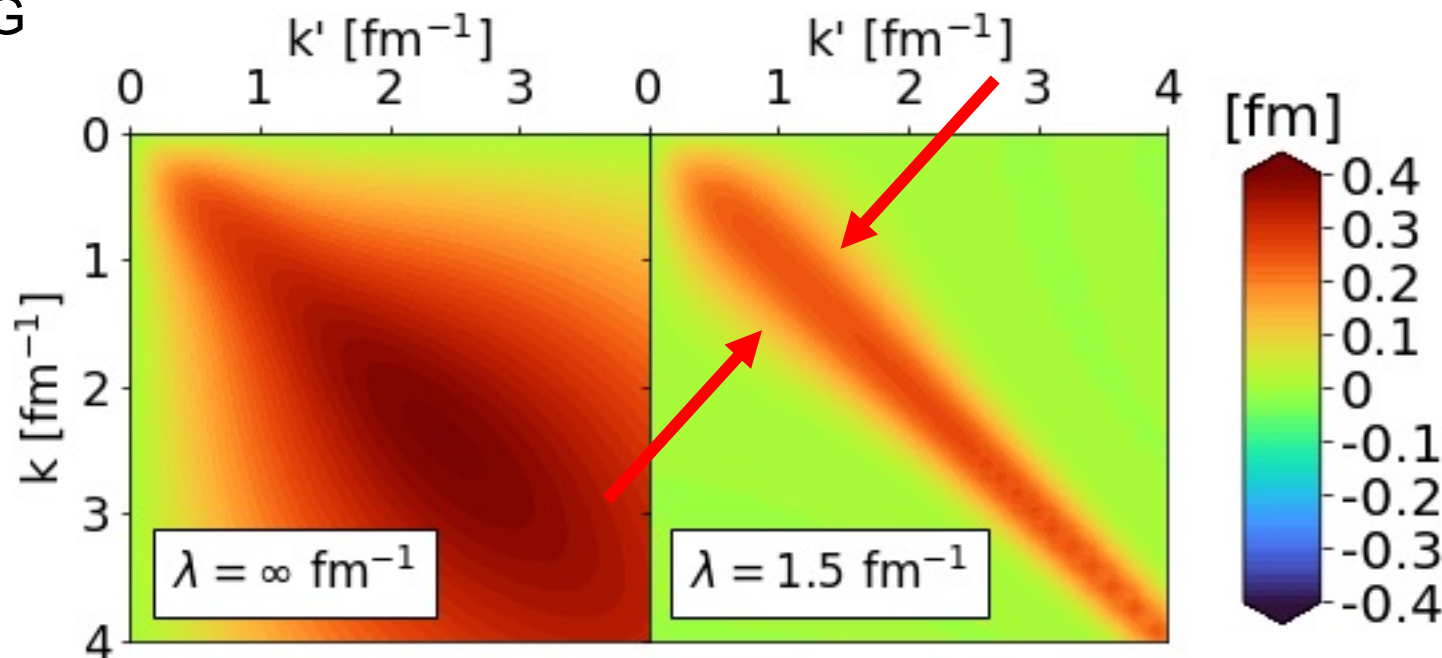


**Fig. 1:** Momentum space matrix elements of Argonne v18 (AV18) under SRG evolution in  ${}^1P_1$  channel.

# Similarity renormalization group

- Evolve to low RG resolution using the SRG

$$O(s) = U(s)O(0)U^\dagger(s)$$

where  $s = 0 \rightarrow \infty$  and  $U(s)$  is unitary

- SRG transformations decouple high- and low-momenta in the Hamiltonian
- In practice, solve differential flow equation

$$\frac{dO(s)}{ds} = [\eta(s), O(s)]$$

where  $\eta(s) \equiv \frac{dU(s)}{ds} U^\dagger(s) = [G, H(s)]$  is the SRG generator

- Decoupling scale given by  $\lambda = s^{-1/4}$

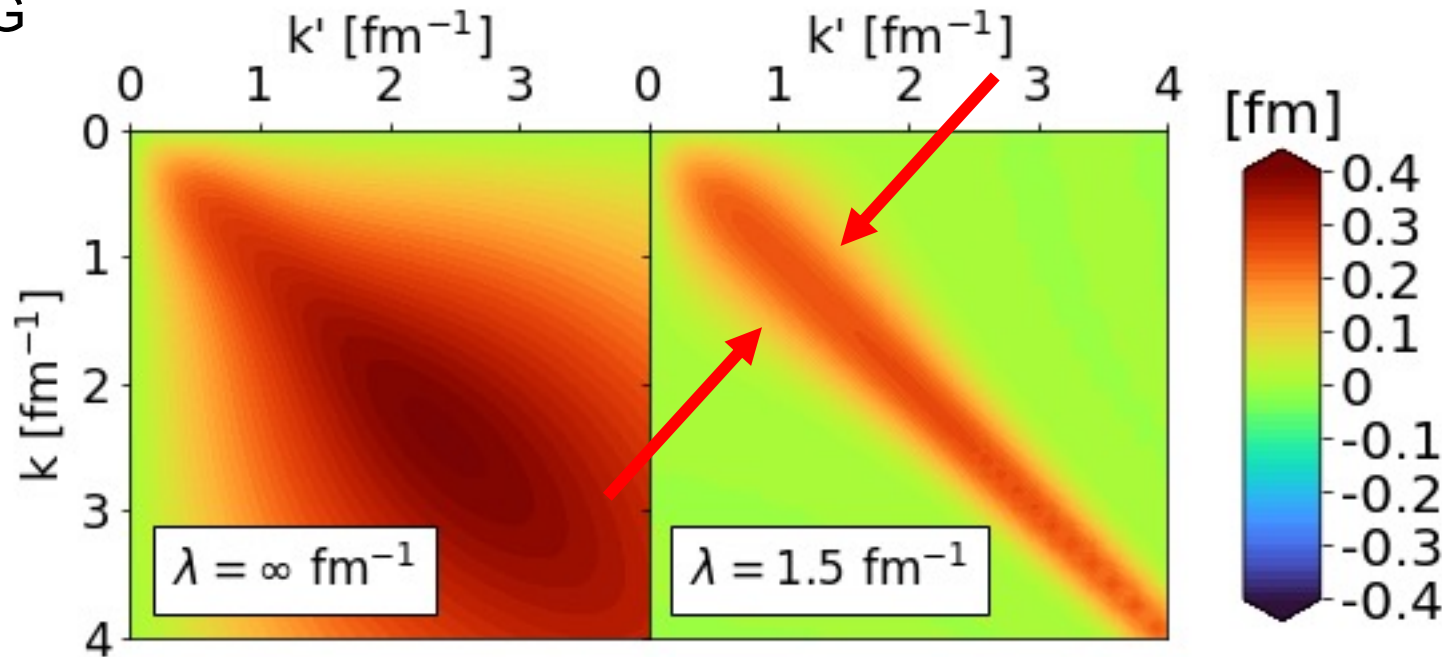


**Fig. 1:** Momentum space matrix elements of Argonne v18 (AV18) under SRG evolution in  ${}^1\text{P}_1$  channel.

# Similarity renormalization group

- AV18 wave function has significant SRC
- What happens to the wave function under SRG transformation?

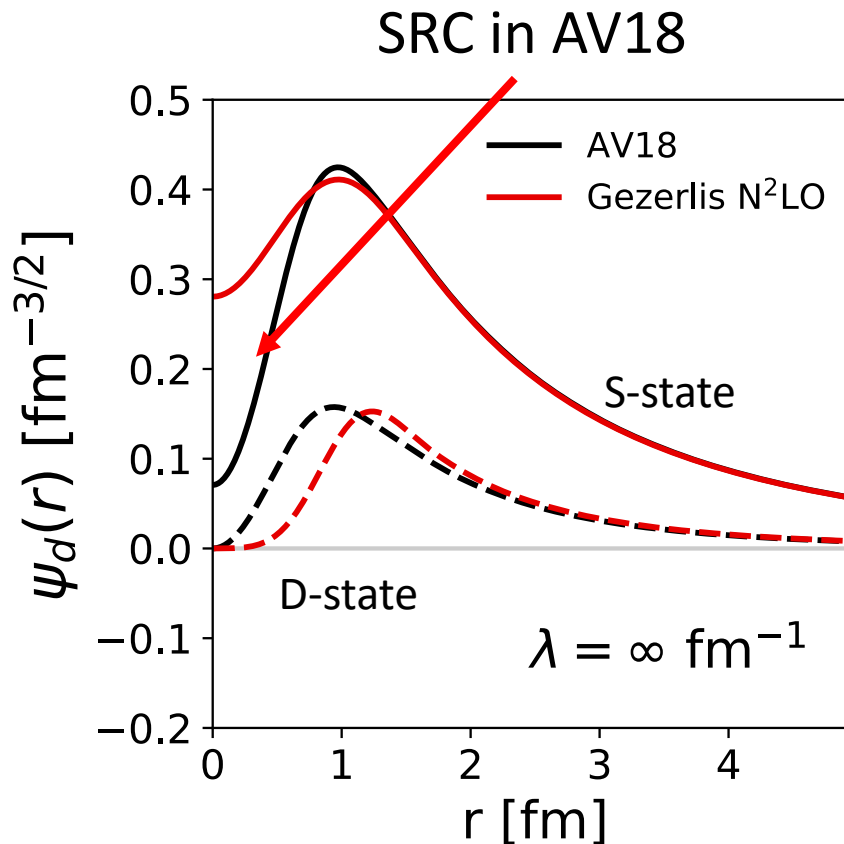


**Fig. 2:** SRG evolution of deuteron wave function in coordinate space for AV18 and Gezerlis  $N^2\text{LO}$ <sup>1</sup>.

# Similarity renormalization group

- SRC physics in AV18 is gone from wave function at low RG resolution
- Deuteron wave functions become soft and D-state probability goes down
- Observables such as asymptotic D-S ratio are the same

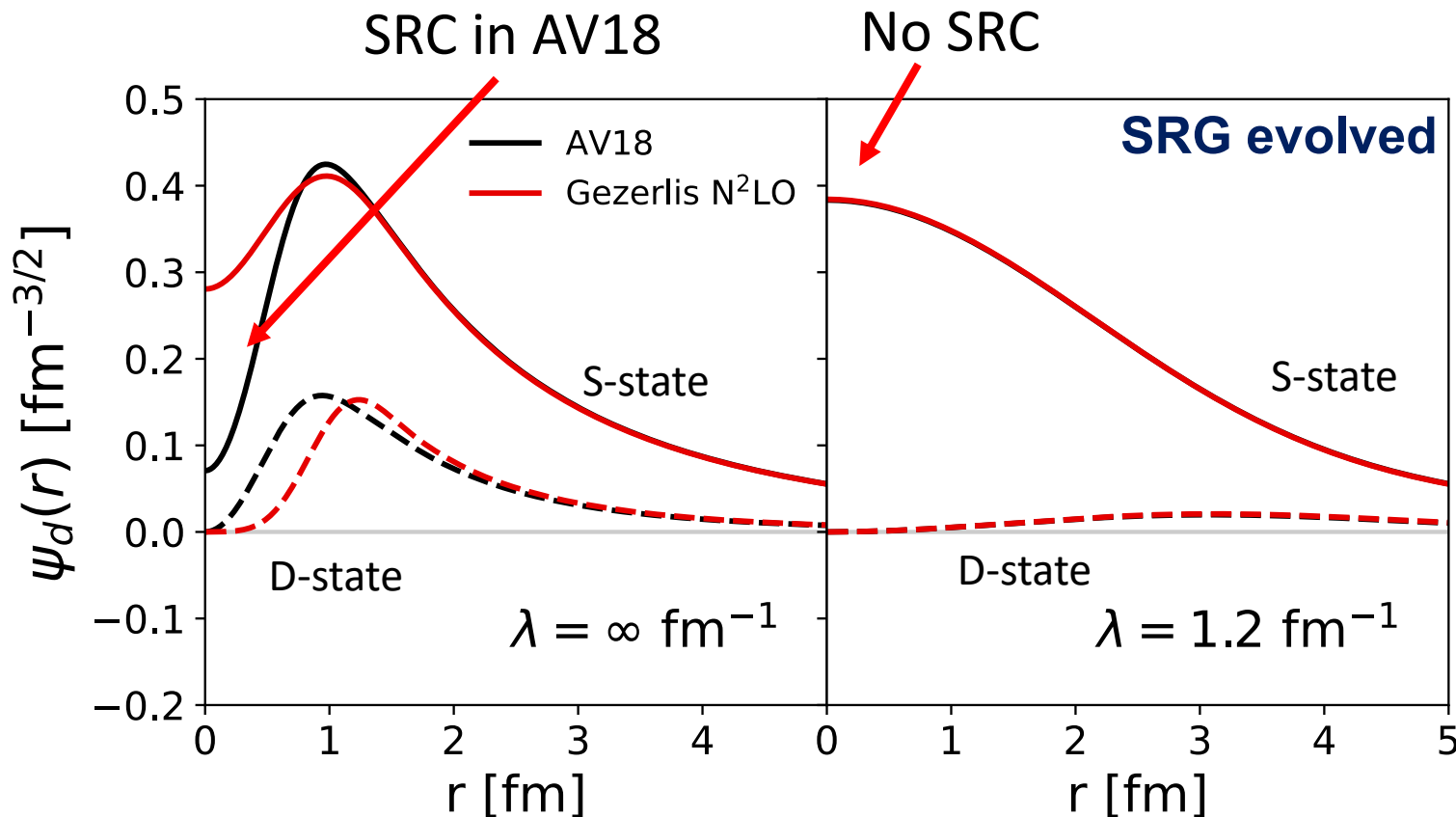


**Fig. 2:** SRG evolution of deuteron wave function in coordinate space for AV18 and Gezerlis N<sup>2</sup>LO<sup>1</sup>.

# Operator evolution

- SRC physics shifts to the operators with soft wave functions at low RG resolution

$$\langle \psi_f^{hi} | U_\lambda^\dagger U_\lambda O^{hi} U_\lambda^\dagger U_\lambda | \psi_i^{hi} \rangle = \langle \psi_f^{low} | O^{low} | \psi_i^{low} \rangle$$

# Operator evolution

- SRC physics shifts to the operators with soft wave functions at low RG resolution

$$\langle \psi_f^{hi} | U_\lambda^\dagger U_\lambda O^{hi} U_\lambda^\dagger U_\lambda | \psi_i^{hi} \rangle = \langle \psi_f^{low} | O^{low} | \psi_i^{low} \rangle$$

- Expand SRG transformation to 2-body level

$$\widehat{U}_\lambda = 1 + \frac{1}{4} \sum_{\mathbf{K}, \mathbf{k}, \mathbf{k}'} \delta U_\lambda^{(2)}(\mathbf{k}, \mathbf{k}') a_{\frac{\mathbf{K}}{2} + \mathbf{k}}^\dagger a_{\frac{\mathbf{K}}{2} - \mathbf{k}}^\dagger a_{\frac{\mathbf{K}}{2} - \mathbf{k}'} a_{\frac{\mathbf{K}}{2} + \mathbf{k}'} + \dots$$

- $\delta U_\lambda^{(2)}$  term is fixed by SRG evolution on  $A = 2$  and inherits the symmetries of  $V_{NN}$

# Operator evolution

- SRC physics shifts to the operators with soft wave functions at low RG resolution

$$\langle \psi_f^{hi} | U_\lambda^\dagger U_\lambda O^{hi} U_\lambda^\dagger U_\lambda | \psi_i^{hi} \rangle = \langle \psi_f^{low} | O^{low} | \psi_i^{low} \rangle$$

- Expand SRG transformation to 2-body level

$$\widehat{U}_\lambda = 1 + \frac{1}{4} \sum_{K, k, k'} \delta U_\lambda^{(2)}(\mathbf{k}, \mathbf{k}') a_{\frac{K}{2}+k}^\dagger a_{\frac{K}{2}-k}^\dagger a_{\frac{K}{2}-k'} a_{\frac{K}{2}+k'} + \dots$$

- $\delta U_\lambda^{(2)}$  term is fixed by SRG evolution on  $A = 2$  and inherits the symmetries of  $V_{NN}$
- For momentum distributions, evolve  $\hat{n}^{hi}(\mathbf{q}) = a_{\mathbf{q}}^\dagger a_{\mathbf{q}}$  and  $\hat{n}^{hi}(\mathbf{q}, \mathbf{Q}) = a_{\frac{\mathbf{Q}}{2}+\mathbf{q}}^\dagger a_{\frac{\mathbf{Q}}{2}-\mathbf{q}}^\dagger a_{\frac{\mathbf{Q}}{2}-\mathbf{q}} a_{\frac{\mathbf{Q}}{2}+\mathbf{q}}$
- **Strategy:** Apply Wick's theorem to evaluate  $\widehat{U}_\lambda \hat{n}^{hi}(\mathbf{q}) \widehat{U}_\lambda^\dagger$  and  $\widehat{U}_\lambda \hat{n}^{hi}(\mathbf{q}, \mathbf{Q}) \widehat{U}_\lambda^\dagger$  truncating 3-body and higher terms

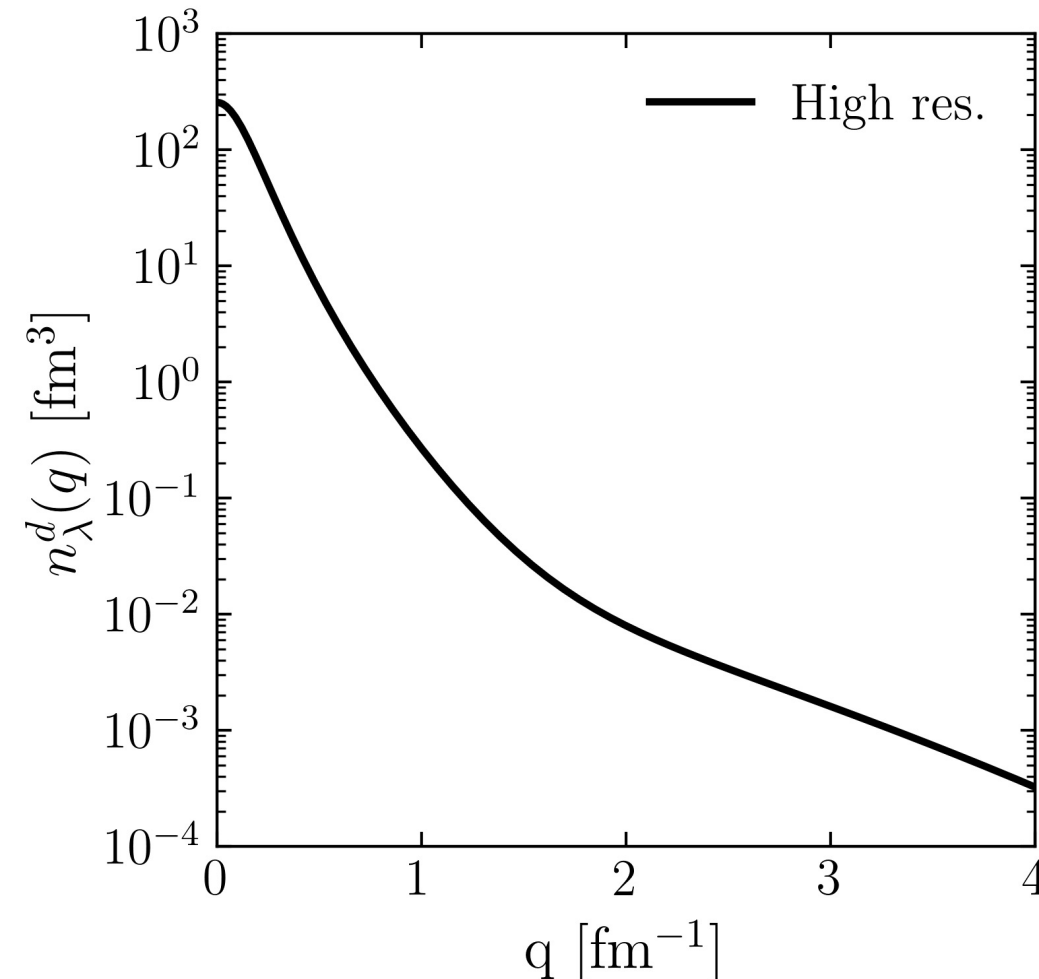
# Momentum distributions at low RG resolution

- **Example:** Evolved single-nucleon momentum distribution

$$\begin{aligned} & \widehat{U}_\lambda \widehat{n}^{hi}(\mathbf{q}) \widehat{U}_\lambda^\dagger \\ & \approx a_{\mathbf{q}}^\dagger a_{\mathbf{q}} + \frac{1}{2} \sum_{\mathbf{K}, \mathbf{k}} [\delta U_\lambda^{(2)} \left( \mathbf{k}, \mathbf{q} - \frac{\mathbf{K}}{2} \right) a_{\frac{\mathbf{K}}{2} + \mathbf{k}}^\dagger a_{\frac{\mathbf{K}}{2} - \mathbf{k}}^\dagger a_{\mathbf{K} - \mathbf{q}} a_{\mathbf{q}} + \delta U_\lambda^{\dagger(2)} \left( \mathbf{q} - \frac{\mathbf{K}}{2}, \mathbf{k} \right) a_{\mathbf{q}}^\dagger a_{\mathbf{K} - \mathbf{q}}^\dagger a_{\frac{\mathbf{K}}{2} - \mathbf{k}}^\dagger a_{\frac{\mathbf{K}}{2} + \mathbf{k}}] \\ & + \frac{1}{4} \sum_{\mathbf{K}, \mathbf{k}, \mathbf{k}'} \delta U_\lambda^{(2)} \left( \mathbf{k}, \mathbf{q} - \frac{\mathbf{K}}{2} \right) \delta U_\lambda^{\dagger(2)} \left( \mathbf{q} - \frac{\mathbf{K}}{2}, \mathbf{k}' \right) a_{\frac{\mathbf{K}}{2} + \mathbf{k}}^\dagger a_{\frac{\mathbf{K}}{2} - \mathbf{k}}^\dagger a_{\frac{\mathbf{K}}{2} - \mathbf{k}'}^\dagger a_{\frac{\mathbf{K}}{2} + \mathbf{k}'}^\dagger \end{aligned}$$

- For operator that probes high momentum ( $q \gg \lambda$ ), the low RG resolution wave function filters out first few terms leaving only  $\delta U \delta U^\dagger$  term

# Momentum distributions at low RG resolution



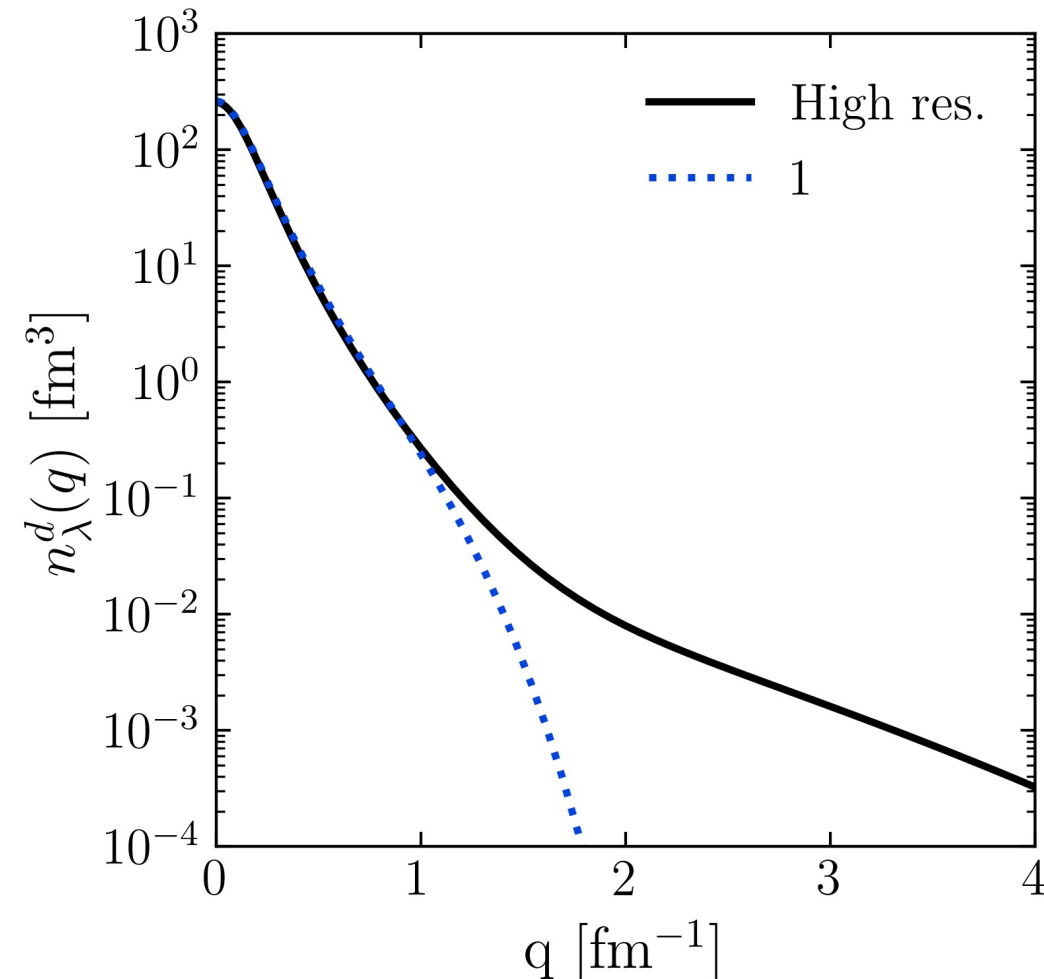
- Deuteron example

$$n^{lo}(\mathbf{q}) = (1 + \delta U) a_{\mathbf{q}}^\dagger a_{\mathbf{q}} (1 + \delta U^\dagger)$$

$$\langle \psi_d^{hi} | a_{\mathbf{q}}^\dagger a_{\mathbf{q}} | \psi_d^{hi} \rangle$$

**Fig. 3:** Contributions to deuteron momentum distribution with AV18 and  $\lambda = 1.35$  fm<sup>-1</sup>.

# Momentum distributions at low RG resolution



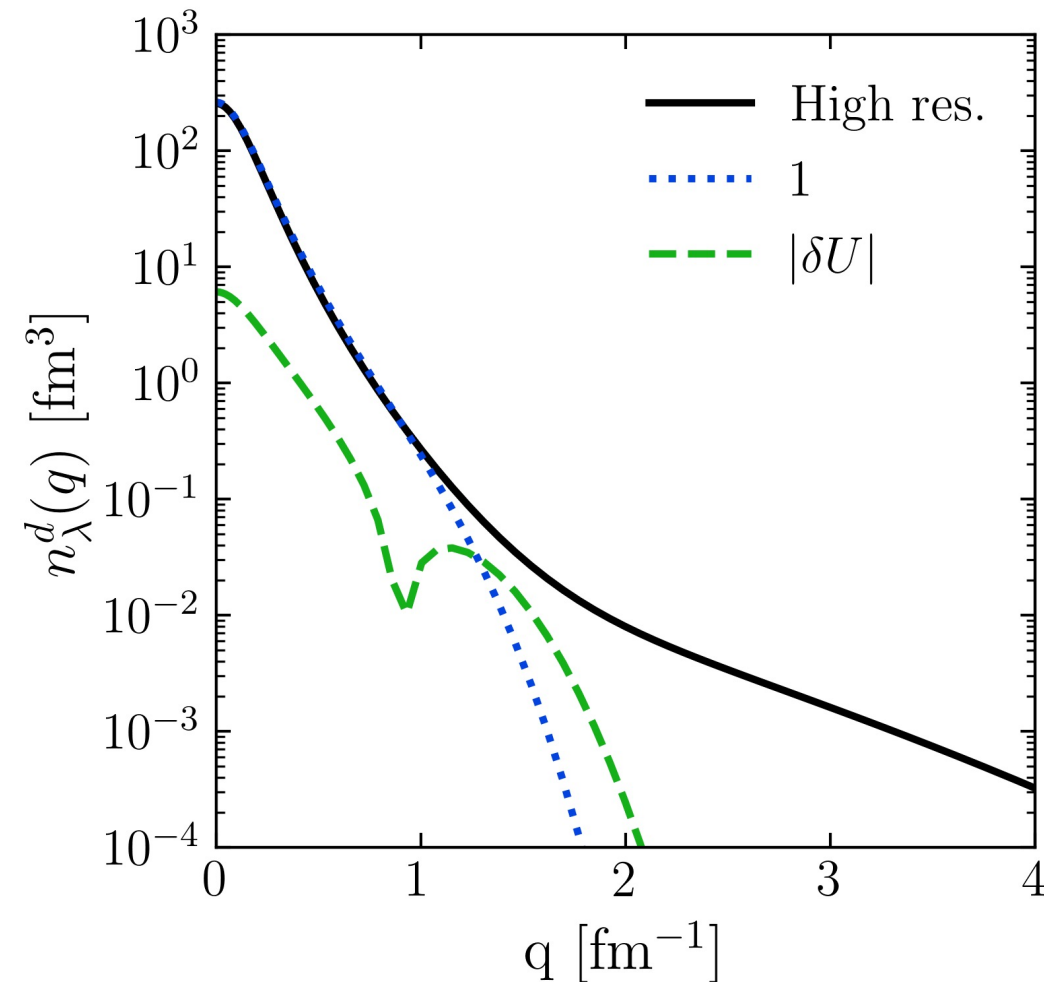
- Deuteron example

$$n^{lo}(\mathbf{q}) = (1 + \delta U) a_{\mathbf{q}}^\dagger a_{\mathbf{q}} (1 + \delta U^\dagger)$$

$$\begin{aligned}\langle \psi_d^{hi} | a_{\mathbf{q}}^\dagger a_{\mathbf{q}} | \psi_d^{hi} \rangle \\ \langle \psi_d^{lo} | a_{\mathbf{q}}^\dagger a_{\mathbf{q}} | \psi_d^{lo} \rangle\end{aligned}$$

**Fig. 3:** Contributions to deuteron momentum distribution with AV18 and  $\lambda = 1.35 \text{ fm}^{-1}$ .

# Momentum distributions at low RG resolution



- Deuteron example

$$n^{lo}(\mathbf{q}) = (1 + \delta U) a_{\mathbf{q}}^\dagger a_{\mathbf{q}} (1 + \delta U^\dagger)$$

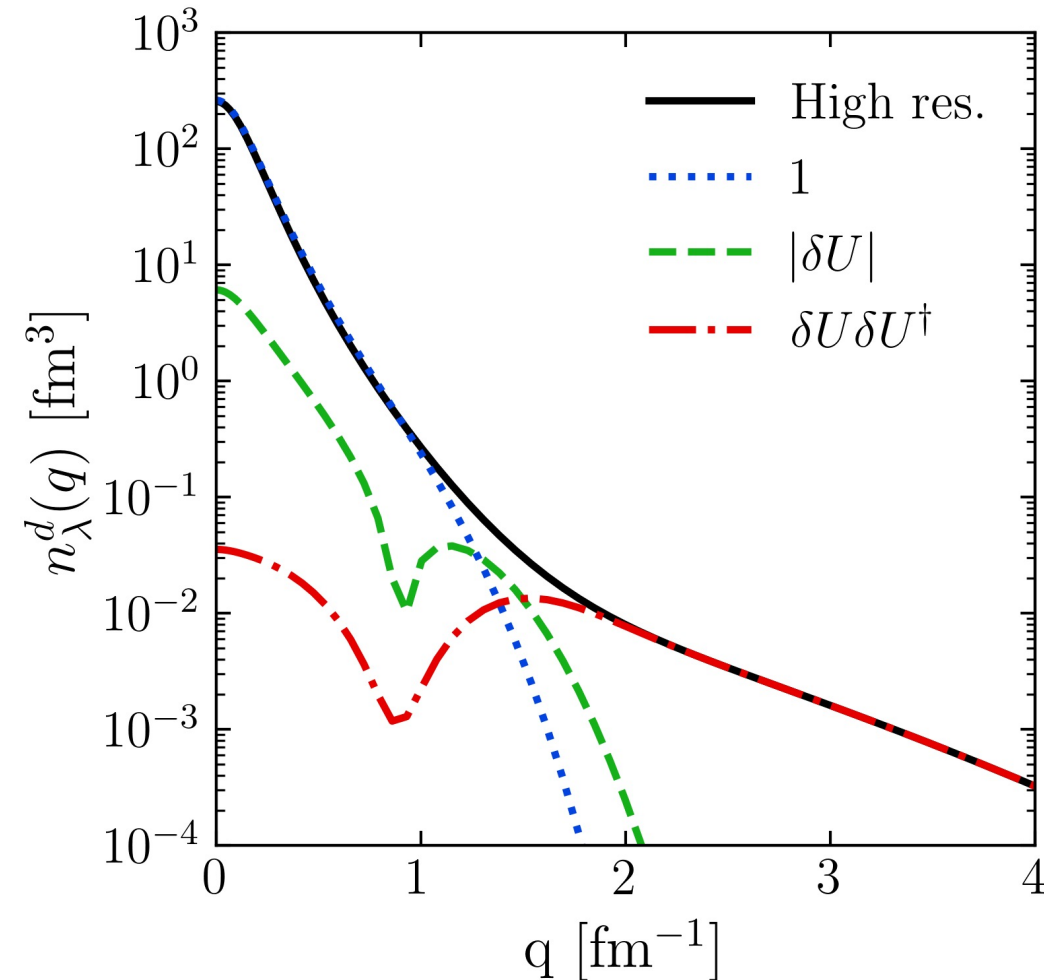
$$\langle \psi_d^{hi} | a_{\mathbf{q}}^\dagger a_{\mathbf{q}} | \psi_d^{hi} \rangle$$

$$\langle \psi_d^{lo} | a_{\mathbf{q}}^\dagger a_{\mathbf{q}} | \psi_d^{lo} \rangle$$

$$\langle \psi_d^{lo} | \delta U a_{\mathbf{q}}^\dagger a_{\mathbf{q}} + a_{\mathbf{q}}^\dagger a_{\mathbf{q}} \delta U^\dagger | \psi_d^{lo} \rangle$$

**Fig. 3:** Contributions to deuteron momentum distribution with AV18 and  $\lambda = 1.35$  fm<sup>-1</sup>.

# Momentum distributions at low RG resolution



- Deuteron example

$$n^{lo}(\mathbf{q}) = (1 + \delta U) a_{\mathbf{q}}^\dagger a_{\mathbf{q}} (1 + \delta U^\dagger)$$

$$\langle \psi_d^{hi} | a_{\mathbf{q}}^\dagger a_{\mathbf{q}} | \psi_d^{hi} \rangle$$

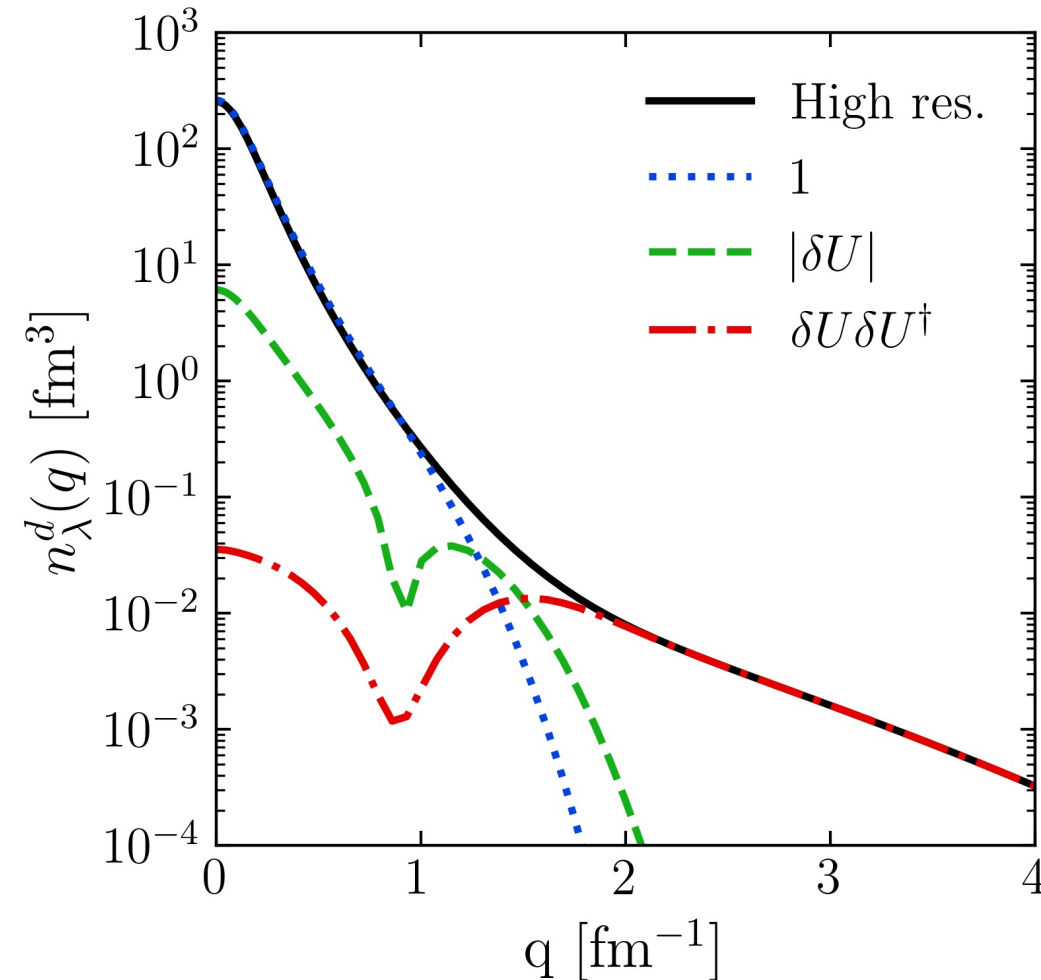
$$\langle \psi_d^{lo} | a_{\mathbf{q}}^\dagger a_{\mathbf{q}} | \psi_d^{lo} \rangle$$

$$\langle \psi_d^{lo} | \delta U a_{\mathbf{q}}^\dagger a_{\mathbf{q}} + a_{\mathbf{q}}^\dagger a_{\mathbf{q}} \delta U^\dagger | \psi_d^{lo} \rangle$$

$$\langle \psi_d^{lo} | \delta U a_{\mathbf{q}}^\dagger a_{\mathbf{q}} \delta U^\dagger | \psi_d^{lo} \rangle$$

**Fig. 3:** Contributions to deuteron momentum distribution with AV18 and  $\lambda = 1.35$  fm<sup>-1</sup>.

# Momentum distributions at low RG resolution

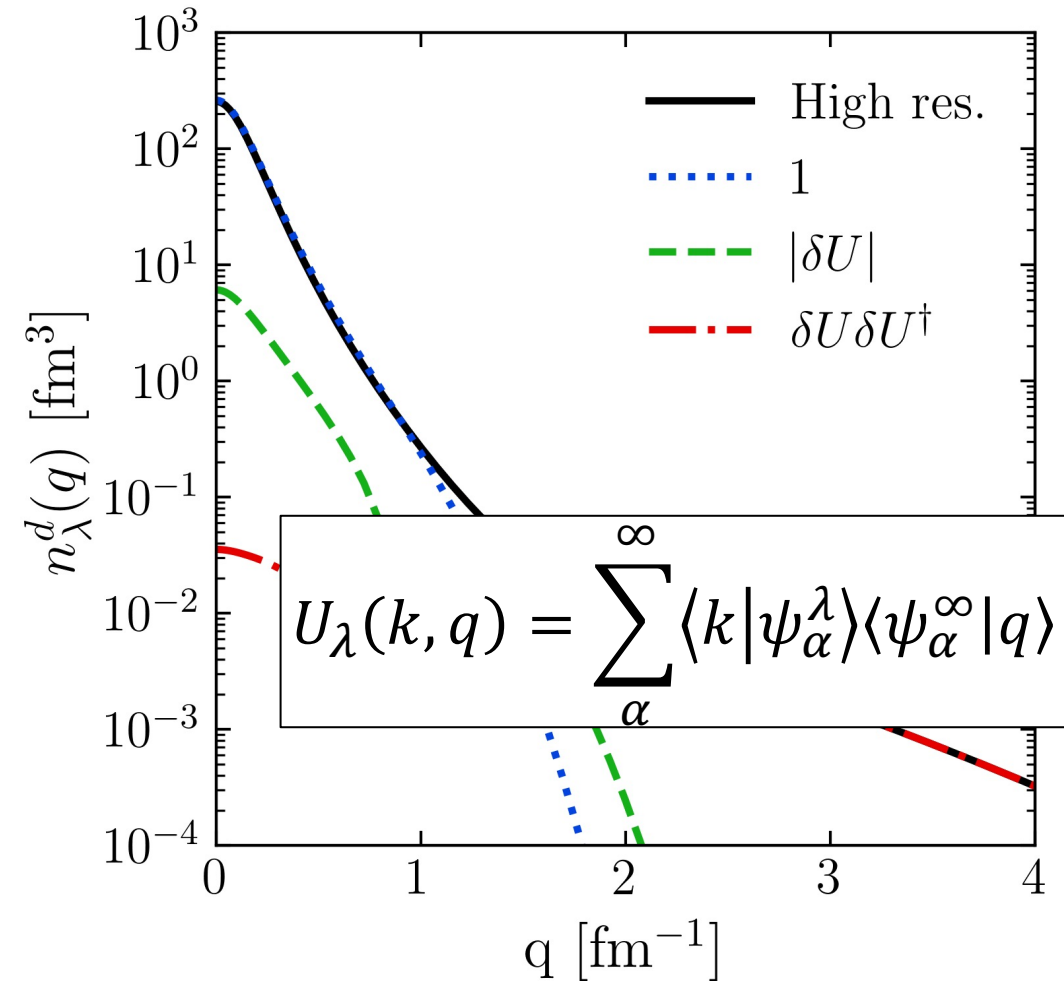


- For high- $q$ , the  $\delta U_\lambda \delta U_\lambda^\dagger$  term dominates

$$\approx \sum_{K,k,k'}^{\lambda} \delta U_\lambda(\mathbf{k}, \mathbf{q}) \delta U_\lambda^\dagger(\mathbf{q}, \mathbf{k}') a_{\mathbf{K}/2 + \mathbf{k}}^\dagger a_{\mathbf{K}/2 - \mathbf{k}}^\dagger a_{\mathbf{K}/2 - \mathbf{k}'} a_{\mathbf{K}/2 + \mathbf{k}'}$$

**Fig. 3:** Contributions to deuteron momentum distribution with AV18 and  $\lambda = 1.35$  fm<sup>-1</sup>.

# Momentum distributions at low RG resolution



- For high- $q$ , the  $\delta U_\lambda \delta U_\lambda^\dagger$  term dominates

$$\approx \sum_{K, k, k'}^\lambda \delta U_\lambda(\mathbf{k}, \mathbf{q}) \delta U_\lambda^\dagger(\mathbf{q}, \mathbf{k}') a_{\frac{\mathbf{K}}{2} + \mathbf{k}}^\dagger a_{\frac{\mathbf{K}}{2} - \mathbf{k}}^\dagger a_{\frac{\mathbf{K}}{2} - \mathbf{k}'} a_{\frac{\mathbf{K}}{2} + \mathbf{k}'}$$

→ **Factorization:**  $\delta U_\lambda(\mathbf{k}, \mathbf{q}) \approx F_\lambda^{lo}(\mathbf{k}) F_\lambda^{hi}(\mathbf{q})$

$$\approx |F_\lambda^{hi}(\mathbf{q})|^2 \sum_{K, k, k'}^\lambda F_\lambda^{lo}(\mathbf{k}) F_\lambda^{lo}(\mathbf{k}') a_{\frac{\mathbf{K}}{2} + \mathbf{k}}^\dagger a_{\frac{\mathbf{K}}{2} - \mathbf{k}}^\dagger a_{\frac{\mathbf{K}}{2} - \mathbf{k}'} a_{\frac{\mathbf{K}}{2} + \mathbf{k}'}$$

**Fig. 3:** Contributions to deuteron momentum distribution with AV18 and  $\lambda = 1.35$  fm<sup>-1</sup>.

# Factorization

- Factorization of SRG transformations imply scaling of high- $q$  tails
- Consider ratio  $\frac{n^A(\mathbf{q})}{n^d(\mathbf{q})}$  for  $q \gg \lambda$ ,

$$\frac{\langle \Psi_\lambda^A | U_\lambda a_q^\dagger a_q U_\lambda^\dagger | \Psi_\lambda^A \rangle}{\langle \Psi_\lambda^d | U_\lambda a_q^\dagger a_q U_\lambda^\dagger | \Psi_\lambda^d \rangle} = \frac{|F_\lambda^{hi}(\mathbf{q})|^2}{|F_\lambda^{hi}(\mathbf{q})|^2} \times \frac{\langle \Psi_\lambda^A | \sum_{\mathbf{K}, \mathbf{k}, \mathbf{k}'} F_\lambda^{lo}(\mathbf{k}) F_\lambda^{lo}(\mathbf{k}') a_{\frac{\mathbf{K}}{2} + \mathbf{k}}^\dagger a_{\frac{\mathbf{K}}{2} - \mathbf{k}}^\dagger a_{\frac{\mathbf{K}}{2} - \mathbf{k}'} a_{\frac{\mathbf{K}}{2} + \mathbf{k}'} | \Psi_\lambda^A \rangle}{\langle \Psi_\lambda^d | \sum_{\mathbf{K}, \mathbf{k}, \mathbf{k}'} F_\lambda^{lo}(\mathbf{k}) F_\lambda^{lo}(\mathbf{k}') a_{\frac{\mathbf{K}}{2} + \mathbf{k}}^\dagger a_{\frac{\mathbf{K}}{2} - \mathbf{k}}^\dagger a_{\frac{\mathbf{K}}{2} - \mathbf{k}'} a_{\frac{\mathbf{K}}{2} + \mathbf{k}'} | \Psi_\lambda^d \rangle}$$

~~$|F_\lambda^{hi}(\mathbf{q})|^2$~~

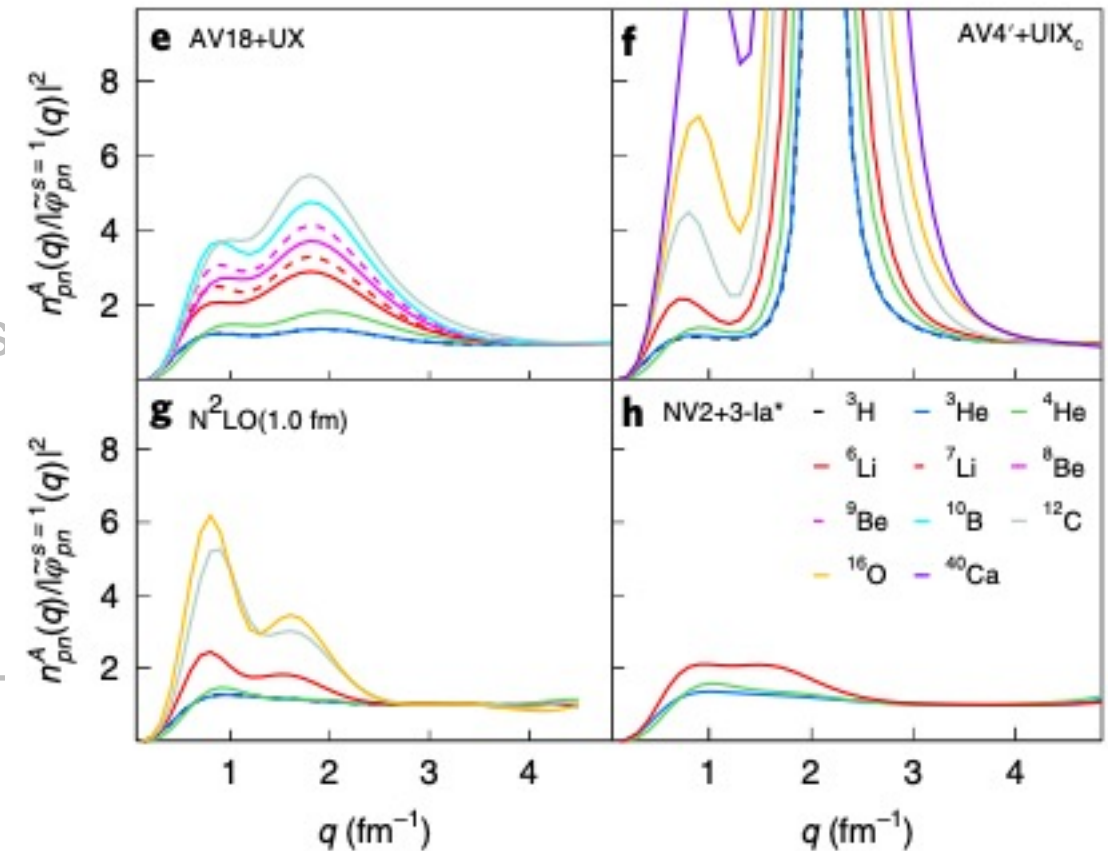
- High- $q$  dependence cancels leaving ratio only sensitive to low-momentum physics

# Factorization

- Factorization of SRG transformations imply s

Factorization built into GCF model seen by flat ratio of pair momentum distributions  $n^A(q)$  over universal two-body wave functions  $|\tilde{\varphi}(q)|^2$  at high- $q$

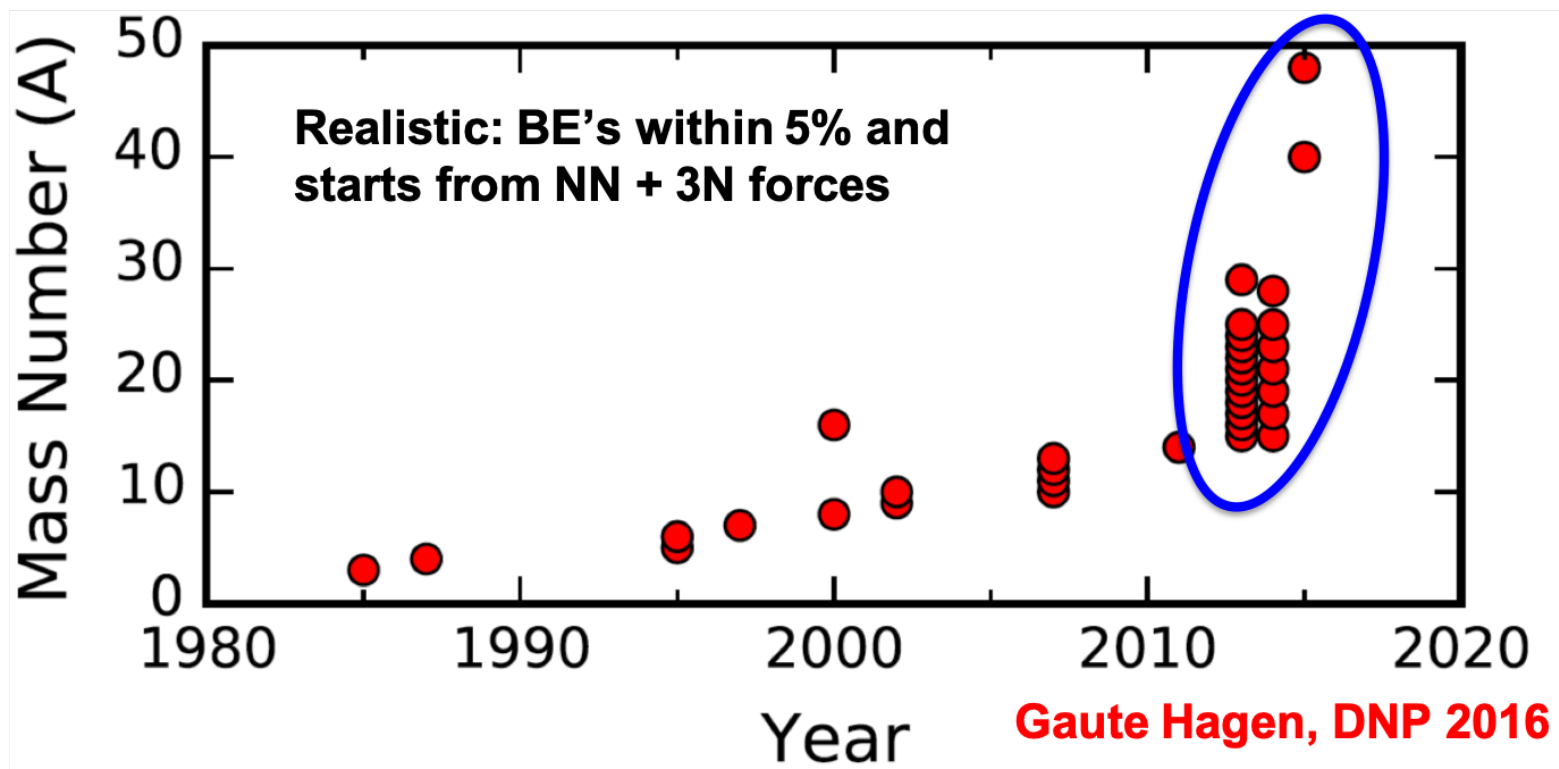
Figure from R. Cruz-Torres et al., Nat. Phys. 17, 306 (2021)



- High- $q$  dependence cancels leaving ratio only sensitive to low-momentum physics

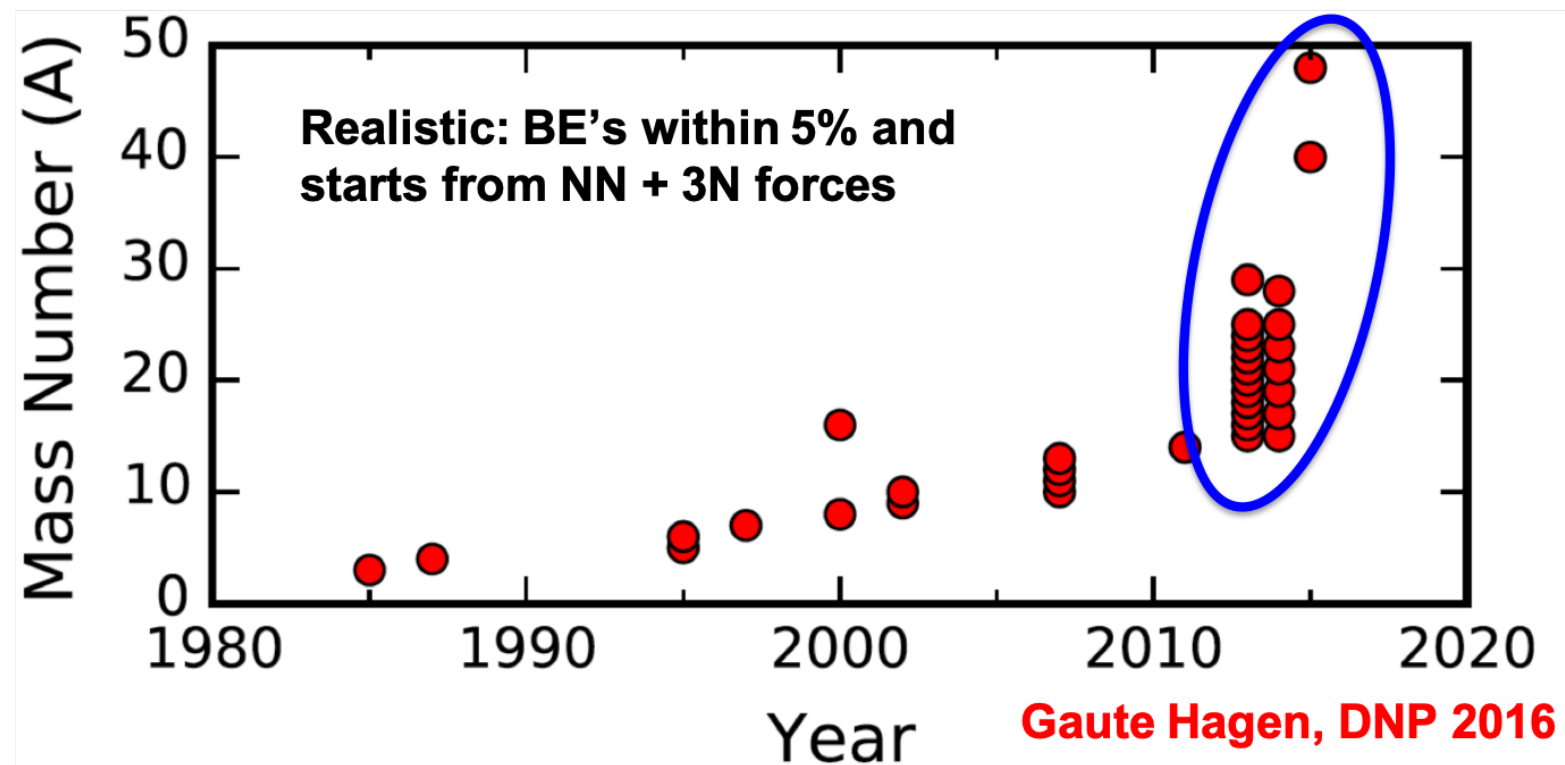
# Why low RG resolution?

- Methods that rely on soft interactions work well!



# Why low RG resolution?

- Methods that rely on soft interactions work well!
- What SRC physics can we describe using simple approximations?
- Try Hartree-Fock (HF) with a local density approximation (LDA) to evaluate nuclear matrix elements



# HF and LDA calculation

- Evaluating SRG-evolved operator with low RG resolution wave functions  $\langle \Psi_\lambda^A | \hat{U}_\lambda \hat{n}^{hi}(\mathbf{q}) \hat{U}_\lambda^\dagger | \Psi_\lambda^A \rangle$

$$\begin{aligned} &\approx \langle \Psi_\lambda^A | \left[ a_{\mathbf{q}}^\dagger a_{\mathbf{q}} + \frac{1}{2} \sum_{\mathbf{K}, \mathbf{k}} \left( \delta U_\lambda(\mathbf{k}, \mathbf{q} - \mathbf{K}/2) a_{\mathbf{K}/2+\mathbf{k}}^\dagger a_{\mathbf{K}/2-\mathbf{k}}^\dagger a_{\mathbf{K}-\mathbf{q}} a_{\mathbf{q}} \right. \right. \\ &\quad \left. \left. + \delta U_\lambda^\dagger(\mathbf{q} - \mathbf{K}/2, \mathbf{k}) a_{\mathbf{q}}^\dagger a_{\mathbf{K}-\mathbf{q}}^\dagger a_{\mathbf{K}/2-\mathbf{k}} a_{\mathbf{K}/2+\mathbf{k}} \right) \right. \\ &\quad \left. + \frac{1}{4} \sum_{\mathbf{K}, \mathbf{k}, \mathbf{k}'} \delta U_\lambda(\mathbf{k}, \mathbf{q} - \mathbf{K}/2) \delta U_\lambda^\dagger(\mathbf{q} - \mathbf{K}/2, \mathbf{k}') a_{\mathbf{K}/2+\mathbf{k}}^\dagger a_{\mathbf{K}/2-\mathbf{k}}^\dagger a_{\mathbf{K}/2-\mathbf{k}'} a_{\mathbf{K}/2+\mathbf{k}'} \right] | \Psi_\lambda^A \rangle \end{aligned}$$

# HF and LDA calculation

- Evaluating SRG-evolved operator with low RG resolution wave functions  $\langle \Psi_\lambda^A | \hat{U}_\lambda \hat{n}^{hi}(\mathbf{q}) \hat{U}_\lambda^\dagger | \Psi_\lambda^A \rangle$

$$\begin{aligned} &\approx \langle \Psi_\lambda^A | \left[ a_{\mathbf{q}}^\dagger a_{\mathbf{q}} + \frac{1}{2} \sum_{\mathbf{K}, \mathbf{k}} \left( \delta U_\lambda(\mathbf{k}, \mathbf{q} - \mathbf{K}/2) a_{\mathbf{K}/2+\mathbf{k}}^\dagger a_{\mathbf{K}/2-\mathbf{k}}^\dagger a_{\mathbf{K}-\mathbf{q}} a_{\mathbf{q}} \right. \right. \\ &\quad \left. \left. + \delta U_\lambda^\dagger(\mathbf{q} - \mathbf{K}/2, \mathbf{k}) a_{\mathbf{q}}^\dagger a_{\mathbf{K}-\mathbf{q}}^\dagger a_{\mathbf{K}/2-\mathbf{k}} a_{\mathbf{K}/2+\mathbf{k}} \right) \right. \\ &\quad \left. + \frac{1}{4} \sum_{\mathbf{K}, \mathbf{k}, \mathbf{k}'} \delta U_\lambda(\mathbf{k}, \mathbf{q} - \mathbf{K}/2) \delta U_\lambda^\dagger(\mathbf{q} - \mathbf{K}/2, \mathbf{k}') a_{\mathbf{K}/2+\mathbf{k}}^\dagger a_{\mathbf{K}/2-\mathbf{k}}^\dagger a_{\mathbf{K}/2-\mathbf{k}'} a_{\mathbf{K}/2+\mathbf{k}'} \right] | \Psi_\lambda^A \rangle \end{aligned}$$

- Take continuum limit (suppressing spin and isospin labels):  $\sum_{\mathbf{k}} \rightarrow \int d\mathbf{k}$

# HF and LDA calculation

- Evaluating SRG-evolved operator with low RG resolution wave functions  $\langle \Psi_\lambda^A | \hat{U}_\lambda \hat{n}^{hi}(\mathbf{q}) \hat{U}_\lambda^\dagger | \Psi_\lambda^A \rangle$

$$\begin{aligned} &\approx \langle \Psi_\lambda^A | \left[ a_{\mathbf{q}}^\dagger a_{\mathbf{q}} + \frac{1}{2} \sum_{\mathbf{K}, \mathbf{k}} \left( \delta U_\lambda(\mathbf{k}, \mathbf{q} - \mathbf{K}/2) a_{\mathbf{K}/2+\mathbf{k}}^\dagger a_{\mathbf{K}/2-\mathbf{k}}^\dagger a_{\mathbf{K}-\mathbf{q}} a_{\mathbf{q}} \right. \right. \\ &\quad \left. \left. + \delta U_\lambda^\dagger(\mathbf{q} - \mathbf{K}/2, \mathbf{k}) a_{\mathbf{q}}^\dagger a_{\mathbf{K}-\mathbf{q}}^\dagger a_{\mathbf{K}/2-\mathbf{k}} a_{\mathbf{K}/2+\mathbf{k}} \right) \right. \\ &\quad \left. + \frac{1}{4} \sum_{\mathbf{K}, \mathbf{k}, \mathbf{k}'} \delta U_\lambda(\mathbf{k}, \mathbf{q} - \mathbf{K}/2) \delta U_\lambda^\dagger(\mathbf{q} - \mathbf{K}/2, \mathbf{k}') a_{\mathbf{K}/2+\mathbf{k}}^\dagger a_{\mathbf{K}/2-\mathbf{k}}^\dagger a_{\mathbf{K}/2-\mathbf{k}'} a_{\mathbf{K}/2+\mathbf{k}'} \right] | \Psi_\lambda^A \rangle \end{aligned}$$

- Take continuum limit (suppressing spin and isospin labels):  $\sum_{\mathbf{k}} \rightarrow \int d\mathbf{k}$
- Evaluate matrix elements assuming  $|\Psi_\lambda^A\rangle$  is occupied up to momentum  $k_F$  averaging over local Fermi momentum  $k_F^\tau(R) = (3\pi^2 \rho^\tau(R))^{1/3}$

$$\langle \Psi_\lambda^A | a_{\frac{\mathbf{K}}{2}+\mathbf{k}}^\dagger a_{\frac{\mathbf{K}}{2}-\mathbf{k}}^\dagger a_{\frac{\mathbf{K}}{2}-\mathbf{k}'} a_{\frac{\mathbf{K}}{2}+\mathbf{k}'} | \Psi_\lambda^A \rangle \approx \int d\mathbf{R} \delta(\mathbf{k}' - \mathbf{k}) \theta(k_F^\tau(R) - |\mathbf{K}/2 + \mathbf{k}|) \theta(k_F^{\tau'}(R) - |\mathbf{K}/2 - \mathbf{k}|)$$

# HF and LDA calculation

- Angle-average to evaluate angular dependence of  $\mathbf{q} \cdot \mathbf{k}$ ,  $\mathbf{q} \cdot \mathbf{K}$ , and  $\mathbf{K} \cdot \mathbf{k}$  (defines angles  $x$ ,  $y$ , and  $z$ )

E.g., 
$$\int_{-1}^1 \frac{dz}{2} \theta(k_F^\tau - |\mathbf{K}/2 + \mathbf{k}|) \theta(k_F^{\tau'} - |\mathbf{K}/2 - \mathbf{k}|) = \begin{cases} 1 & \text{if } k < k_F^{\min} - \frac{K}{2} \\ \frac{(k_F^{\min})^2 - (k - K/2)^2}{2kK} & \text{if } k < k_F^{\min} + \frac{K}{2} \text{ and} \\ & k_F^{\min} - \frac{K}{2} < k < k_F^{\max} - \frac{K}{2} \\ \frac{(k_F^{\text{avg}})^2 - k^2 - K^2/4}{kK} & \text{if } k_F^{\max} - \frac{K}{2} < k \text{ and} \\ & k < \sqrt{(k_F^{\text{avg}})^2 - \frac{K^2}{4}} \\ 0 & \text{otherwise} \end{cases}$$
 where  $\left| \frac{\mathbf{K}}{2} + \mathbf{k} \right| = \sqrt{\frac{K^2}{4} + k^2 + Kkz}$

# HF and LDA calculation

- Angle-average to evaluate angular dependence of  $\mathbf{q} \cdot \mathbf{k}$ ,  $\mathbf{q} \cdot \mathbf{K}$ , and  $\mathbf{K} \cdot \mathbf{k}$  (defines angles  $x$ ,  $y$ , and  $z$ )

E.g., 
$$\int_{-1}^1 \frac{dz}{2} \theta(k_F^\tau - |\mathbf{K}/2 + \mathbf{k}|) \theta(k_F^{\tau'} - |\mathbf{K}/2 - \mathbf{k}|) = \begin{cases} 1 & \text{if } k < k_F^{\min} - \frac{K}{2} \\ \frac{(k_F^{\min})^2 - (k - K/2)^2}{2kK} & \text{if } k < k_F^{\min} + \frac{K}{2} \text{ and} \\ & k_F^{\min} - \frac{K}{2} < k < k_F^{\max} - \frac{K}{2} \\ \frac{(k_F^{\text{avg}})^2 - k^2 - K^2/4}{kK} & \text{if } k_F^{\max} - \frac{K}{2} < k \text{ and} \\ & k < \sqrt{(k_F^{\text{avg}})^2 - \frac{K^2}{4}} \\ 0 & \text{otherwise} \end{cases}$$

where  $\left| \frac{\mathbf{K}}{2} + \mathbf{k} \right| = \sqrt{\frac{K^2}{4} + k^2 + Kkz}$

- Finally write in terms of partial waves using

$$|\mathbf{k}_1 \sigma_1 \tau_1 \mathbf{k}_2 \sigma_2 \tau_2\rangle = \frac{1}{\sqrt{2}} \sum_{S,M_S} \sum_{L,M_L} \sum_{J,M_J} \sum_{T,M_T} \langle \sigma_1 \sigma_2 | S M_S \rangle \langle \tau_1 \tau_2 | T M_T \rangle \sqrt{\frac{2}{\pi}} Y_{L,M_L}^*(\hat{k}) \langle LM_L S M_S | J M_J \rangle [1 - (-1)^{L+S+T}] |\mathbf{K} k(LS) J M_J T M_T\rangle$$

where  $\mathbf{k} \equiv \frac{1}{2}(\mathbf{k}_1 - \mathbf{k}_2)$  and  $\mathbf{K} \equiv \mathbf{k}_1 + \mathbf{k}_2$

# HF and LDA calculation

- Final formula for single-nucleon momentum distribution (where  $\tau$  specifies proton or neutron) given by:

$$\begin{aligned} n_\lambda^\tau(q) = & \int d^3R \left\{ 2\theta(k_{\text{F}}^\tau - q) + 32 \sum'_{L,S,T} \sum_J (2J+1) \frac{2}{\pi} \int_0^\infty dk k^2 (k(LS)JT | \delta U | k(LS)JT) \sum_{\tau'} |\langle \tau \tau' | T \tau + \tau' \rangle|^2 \theta(k_{\text{F}}^\tau - q) \right. \\ & \times \int_{-1}^1 \frac{dx}{2} \theta(k_{\text{F}}^{\tau'} - |\mathbf{q} - 2\mathbf{k}|) + 2 \sum'_{L,L',S,T} \sum_J (2J+1) \left( \frac{2}{\pi} \right)^2 \int_0^\infty dk k^2 \int_0^\infty dK K^2 \int_{-1}^1 \frac{dy}{2} \\ & \times \int_{-1}^1 \frac{dz}{2} (k(LS)JT | \delta U | |\mathbf{q} - \mathbf{K}/2| (L'S)JT) (|\mathbf{q} - \mathbf{K}/2| (L'S)JT | \delta U^\dagger | k(LS)JT) \\ & \left. \times \sum_{\tau'} |\langle \tau \tau' | T \tau + \tau' \rangle|^2 \theta(k_{\text{F}}^\tau - |\mathbf{K}/2 + \mathbf{k}|) \theta(k_{\text{F}}^{\tau'} - |\mathbf{K}/2 - \mathbf{k}|) \right\}, \end{aligned}$$

# Proton momentum distributions

- Low RG resolution calculations reproduce momentum distributions of AV18 VMC calculations<sup>1</sup> (high RG resolution)

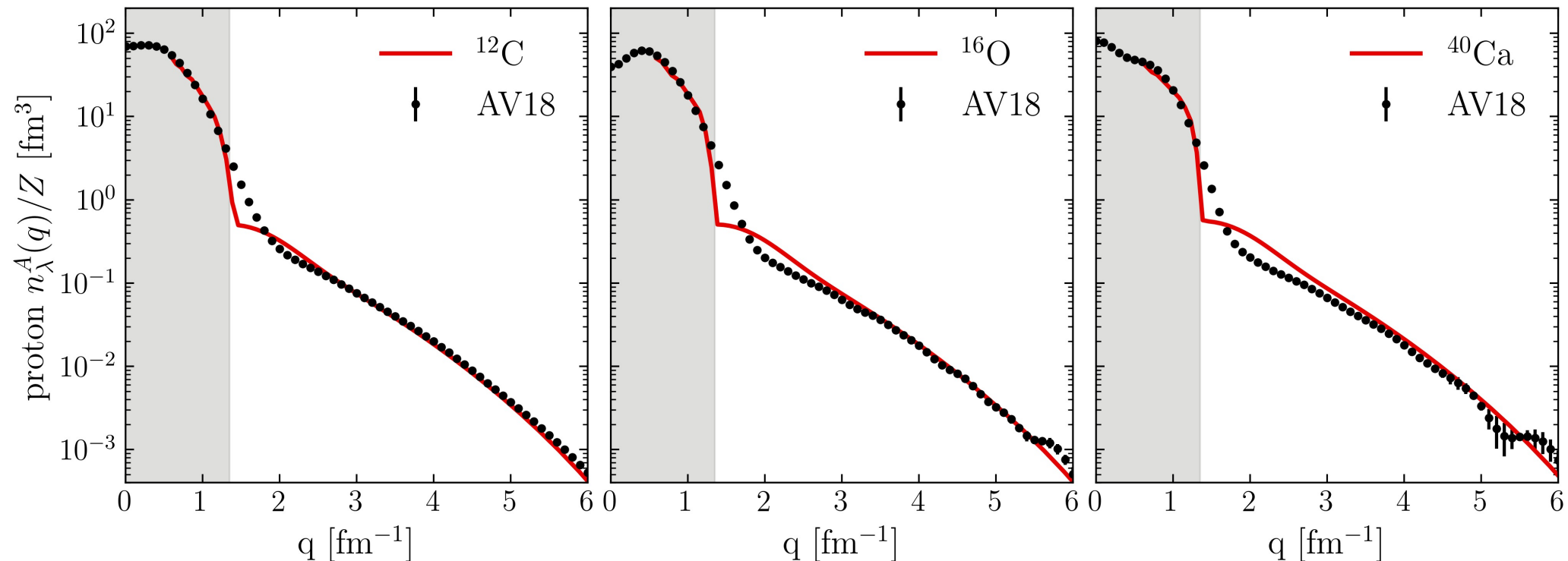


**Fig. 4:** Proton momentum distributions for  $^{12}\text{C}$ ,  $^{16}\text{O}$ , and  $^{40}\text{Ca}$  under HF+LDA with AV18,  $\lambda = 1.35$  fm<sup>-1</sup>, and densities from Skyrme EDF SLy4 using the HFBRAD code<sup>2</sup>.

# Proton momentum distributions

- Low RG resolution calculations reproduce momentum distributions of AV18 VMC calculations<sup>1</sup> (high RG resolution)

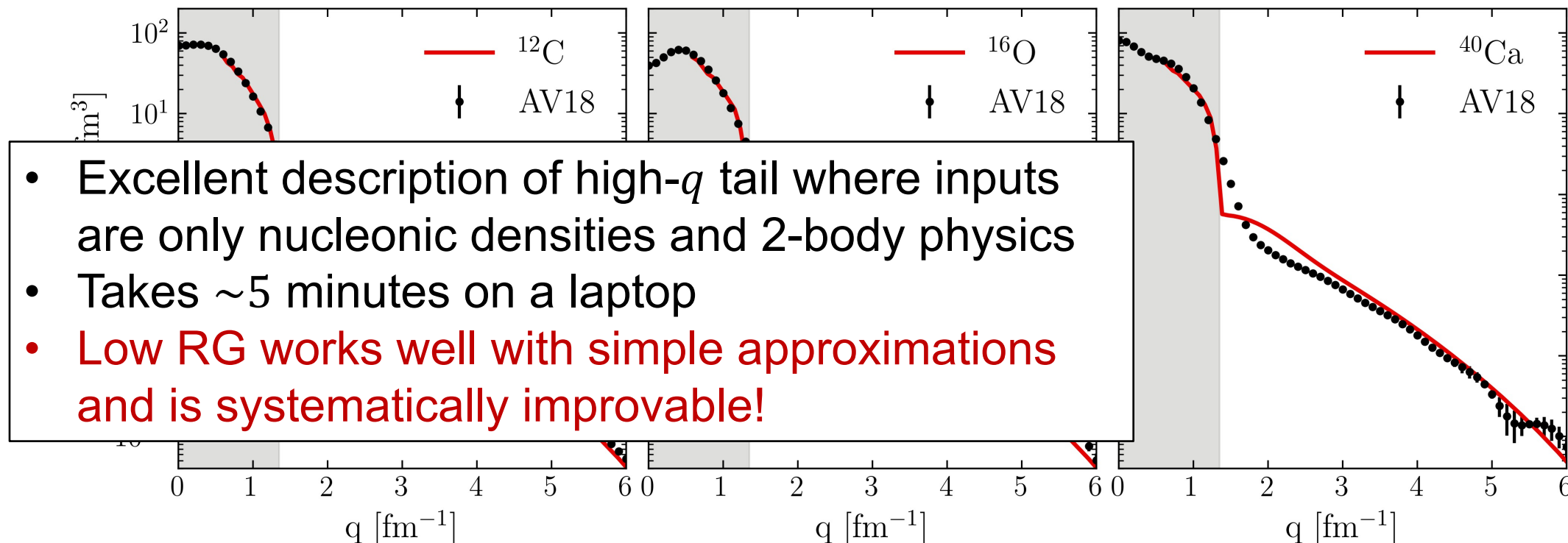
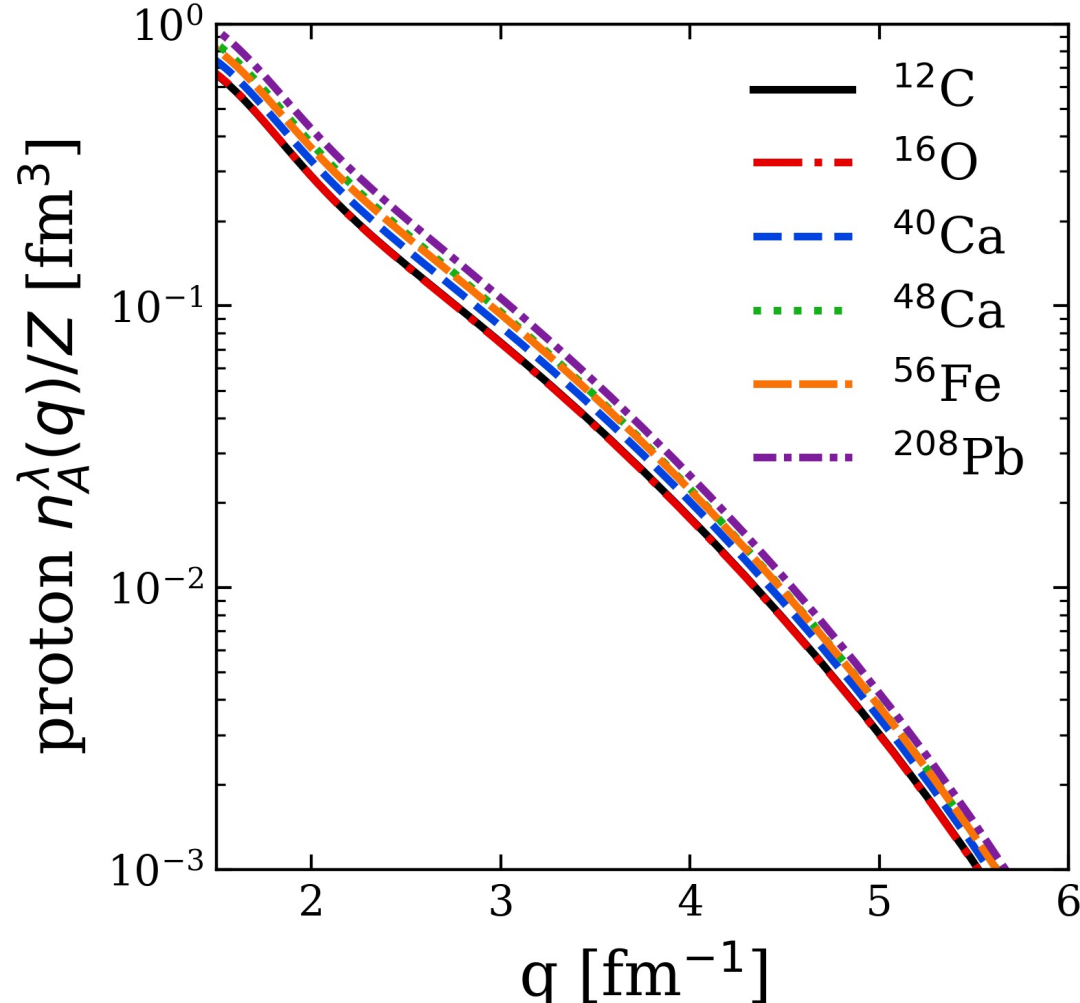


**Fig. 4:** Proton momentum distributions for  $^{12}\text{C}$ ,  $^{16}\text{O}$ , and  $^{40}\text{Ca}$  under HF+LDA with AV18,  $\lambda = 1.35 \text{ fm}^{-1}$ , and densities from Skyrme EDF SLy4 using the HFBRAD code<sup>2</sup>.

# Proton momentum distributions



- **Universality:** High- $q$  dependence from universal function  $\approx |F_\lambda^{hi}(q)|^2$  fixed by 2-body and insensitive to nucleus

**Fig. 5:** Proton momentum distributions under HF+LDA with AV18 and  $\lambda = 1.35 \text{ fm}^{-1}$ , showing several nuclei.

# Proton momentum distributions

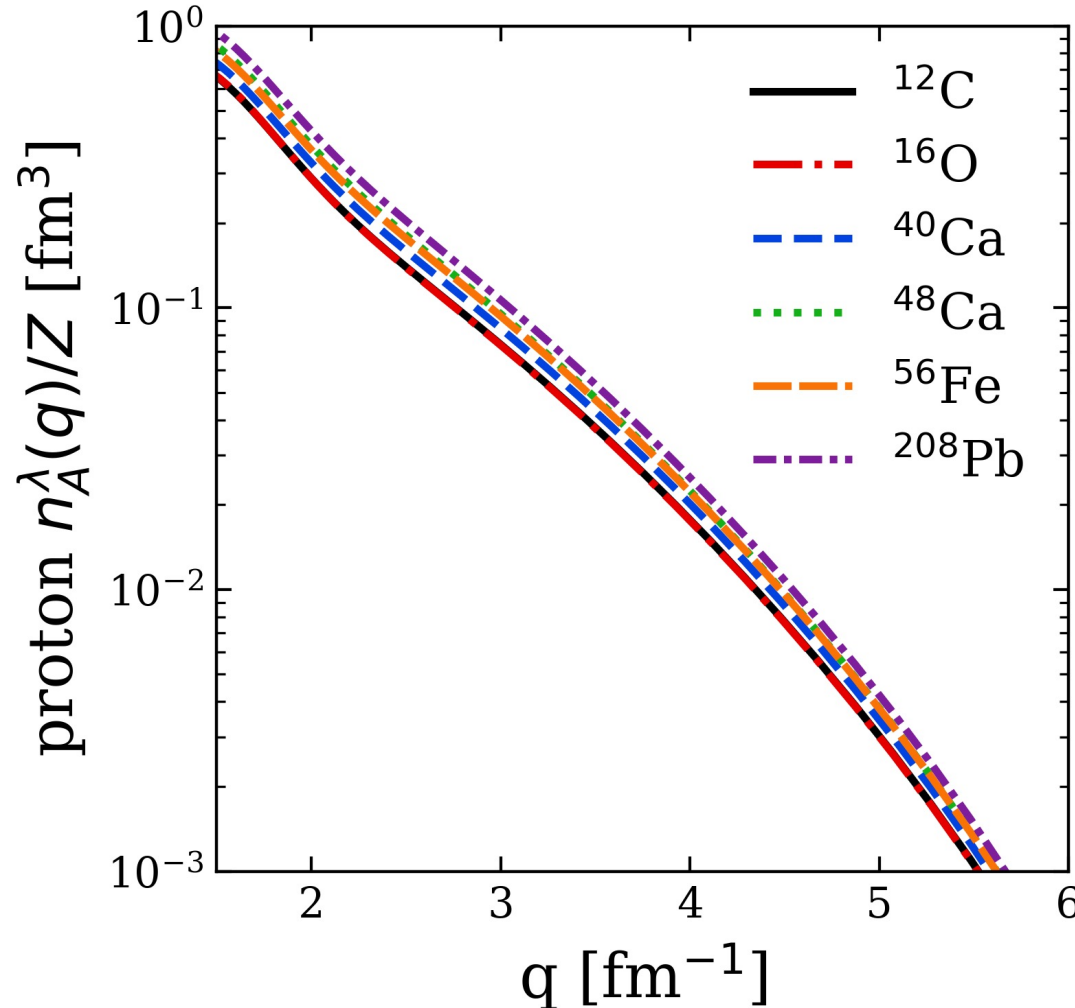
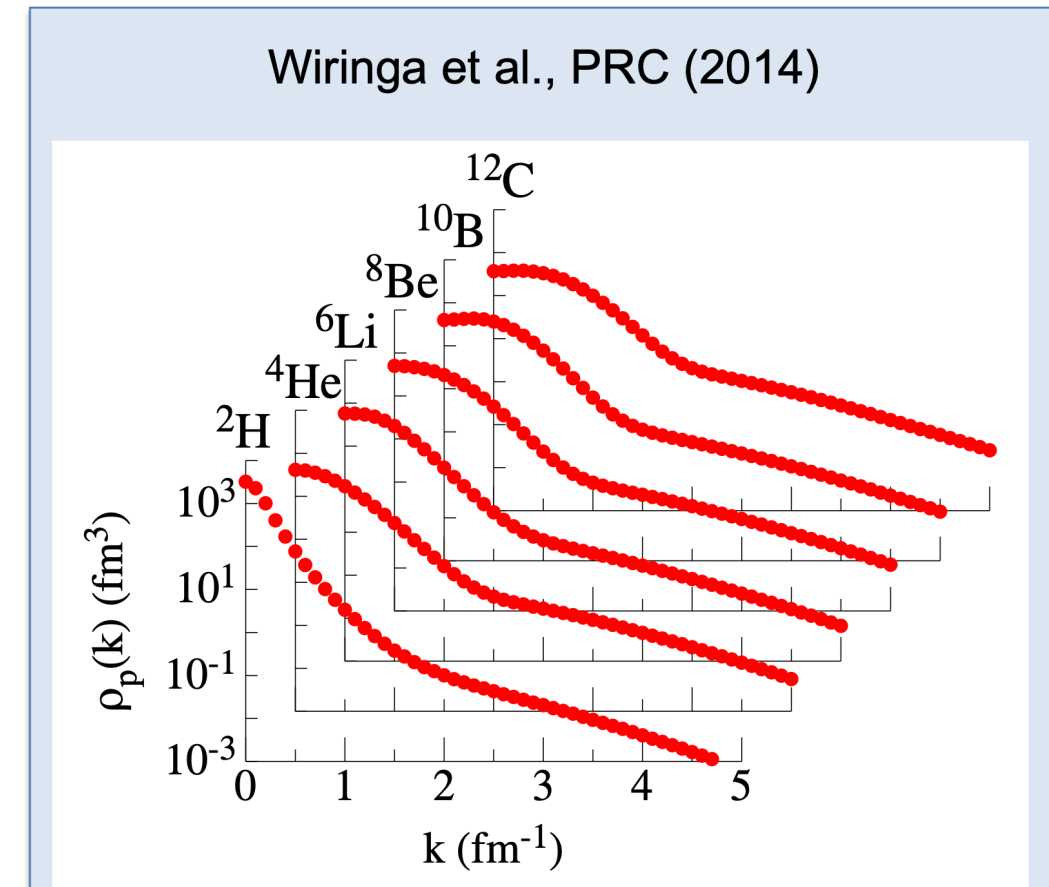


**Fig. 5:** Proton momentum distributions under HF+LDA with AV18 and  $\lambda = 1.35 \text{ fm}^{-1}$ , showing several nuclei.



Consistent with universal high- $q$  tails from VMC calculations of R. B. Wiringa et al., Phys. Rev. C **89**, 024305 (2014)

# SRC scaling factors

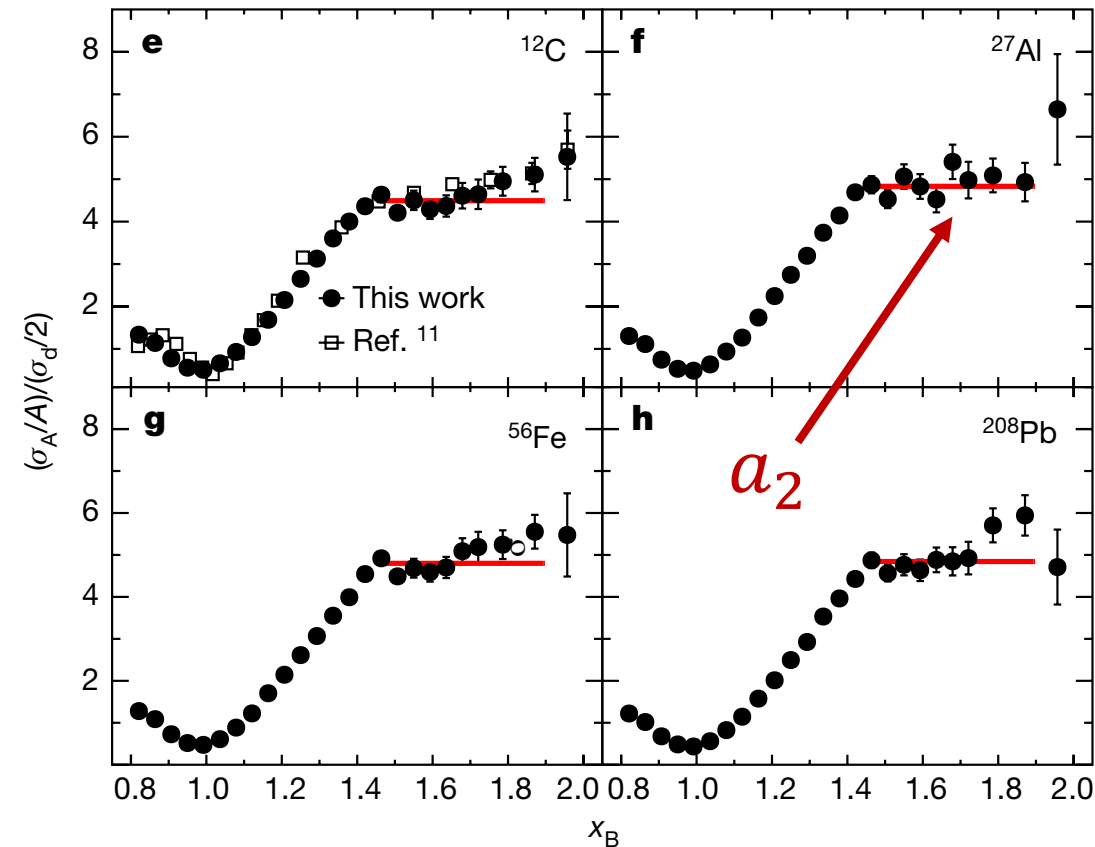


**Fig. 6:** Ratio of per-nucleon electron scattering cross section of nucleus A to that of deuterium, where the red line indicates a constant fit. Figure from B. Schmookler et al. (CLAS), Nature **566**, 354 (2019).

- SRC scaling factors  $a_2$  defined by plateau in cross section ratio  $\frac{2\sigma_A}{A\sigma_d}$  at  $1.45 \leq x \leq 1.9$
- Closely related to the ratio of bound-nucleon probability distributions in the limits of vanishing relative distance (infinitely high relative momentum)
- Extract  $a_2$  from momentum distributions

$$a_2 = \lim_{q \rightarrow \infty} \frac{P^A(q)}{P^d(q)} \approx \frac{\int_{\Delta q^{high}} dq P^A(q)}{\int_{\Delta q^{high}} dq P^d(q)}$$

where  $P^A(q)$  is the single-nucleon probability distribution in nucleus A

# SRC scaling factors

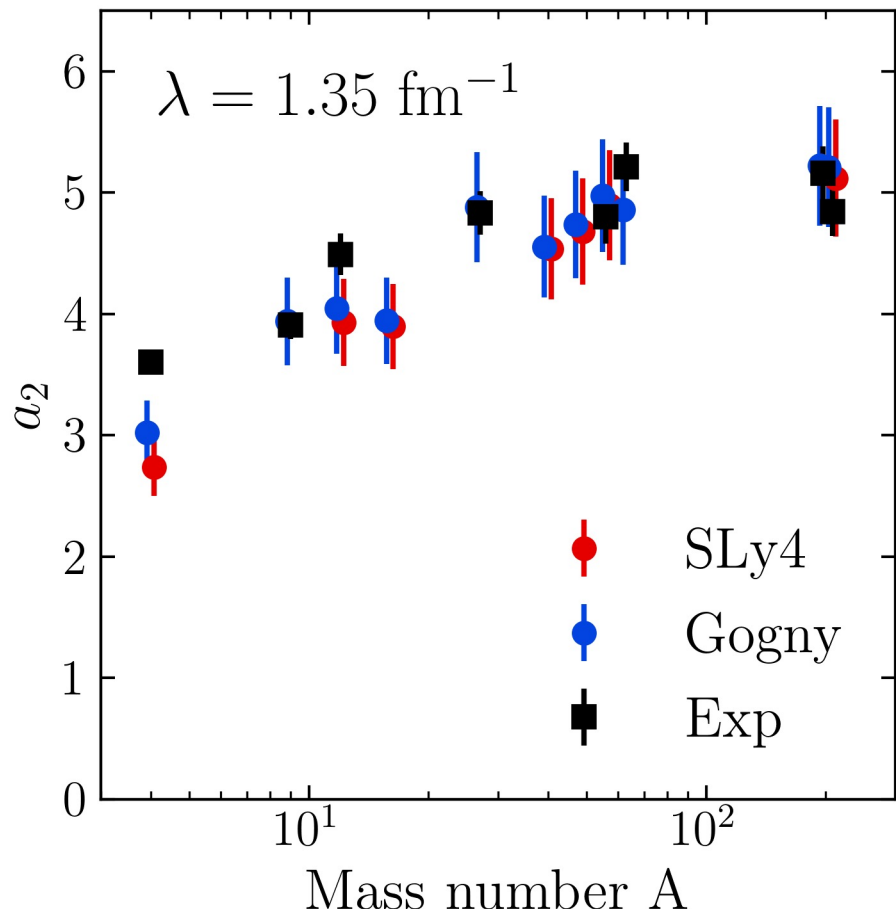


**Fig. 7:**  $a_2$  scale factors using single-nucleon momentum distributions under HF+LDA (SLy4 in red<sup>1</sup>, Gogny<sup>2</sup> in blue) with AV18 and  $\lambda = 1.35 \text{ fm}^{-1}$  compared to experimental values<sup>3</sup>.

$$a_2 = \lim_{q \rightarrow \infty} \frac{P^A(q)}{P^d(q)} \approx \frac{\int_{\Delta q^{high}} dq P^A(q)}{\int_{\Delta q^{high}} dq P^d(q)}$$

- High momentum behavior is characterized by 2-body  $|F_\lambda^{hi}(q)|^2$  which cancels leaving ratio of mean-field (low- $k$ ) physics
- Good agreement with  $a_2$  values from experiment<sup>3</sup> and LCA calculations<sup>4</sup> using two different EDFs
- Error bars from varying  $\Delta q^{high}$

# SRC phenomenology

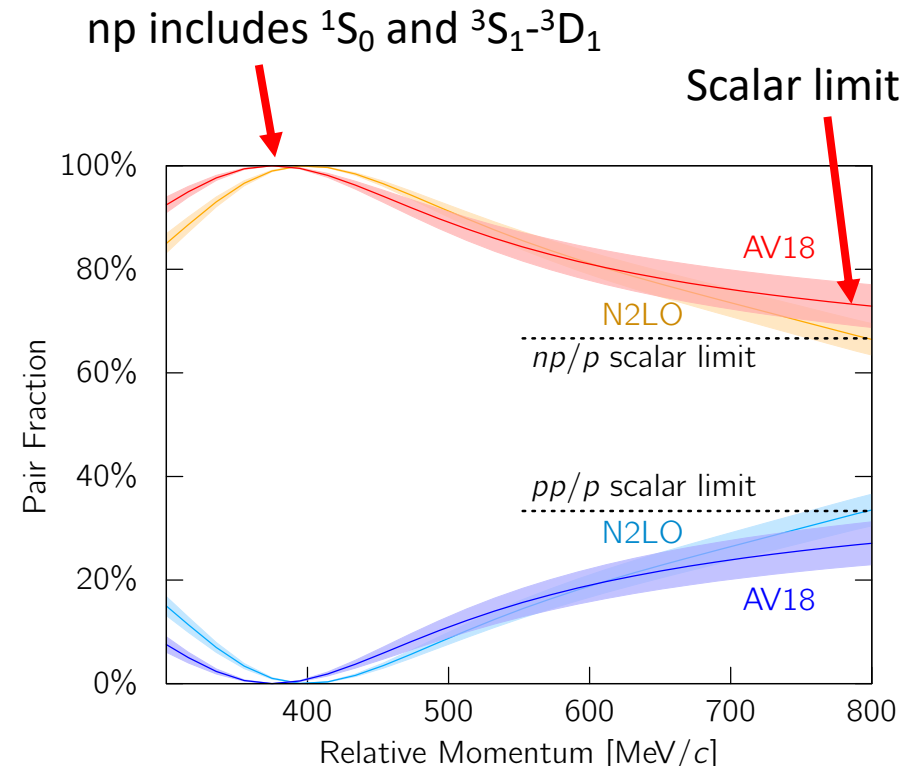
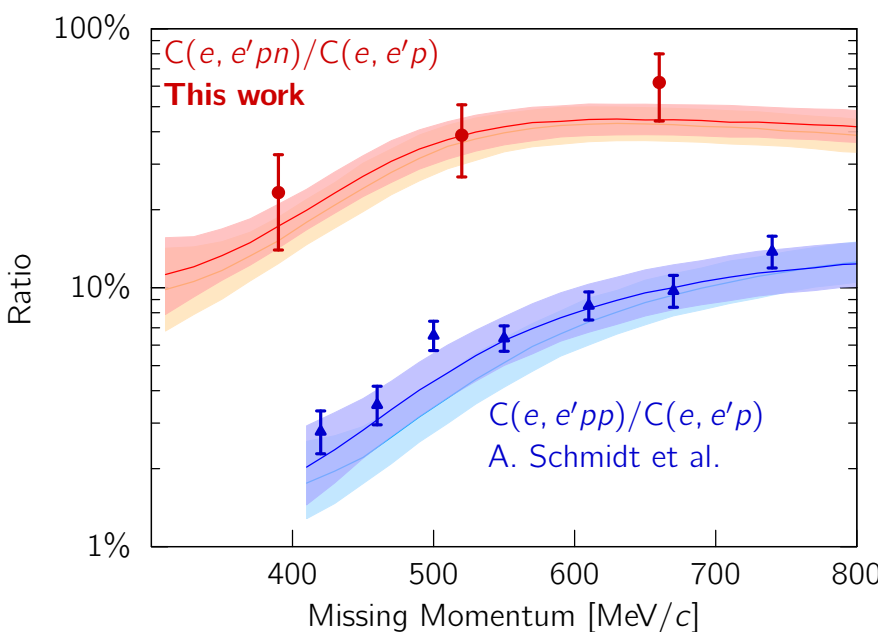


**Fig. 8:** (a) Ratio of two-nucleon to single-nucleon electron-scattering cross sections for carbon as a function of missing momentum. (b) Fraction of np to p and pp to p pairs versus the relative momentum. Figure from CLAS collaboration publication<sup>1</sup>.

- At **high RG resolution**, the tensor force and the repulsive core of the NN interaction kicks nucleon pairs into SRCs
- np dominates because the tensor force requires spin triplet pairs, whereas pp are spin singlets
- **Do we describe this physics at low RG resolution?**

<sup>1</sup>I. Korover et al. (CLAS), arXiv:2004.07304 (2014)

# SRC phenomenology

- At **low RG resolution**, SRCs are suppressed in the wave function and shifted into the operator

$$\hat{n}^{lo}(\mathbf{q}) = \hat{U}_\lambda a_\mathbf{q}^\dagger a_\mathbf{q} \hat{U}_\lambda^\dagger = U_\lambda(\mathbf{k}, \mathbf{q}) U_\lambda^\dagger(\mathbf{q}, \mathbf{k}')$$

- Take ratio of  $^3S_1$  and  $^1S_0$  SRG transformations fixing low-momenta to  $k_0 = 0.1 \text{ fm}^{-1}$
- This physics is established in the 2-body system – can apply to any nucleus!

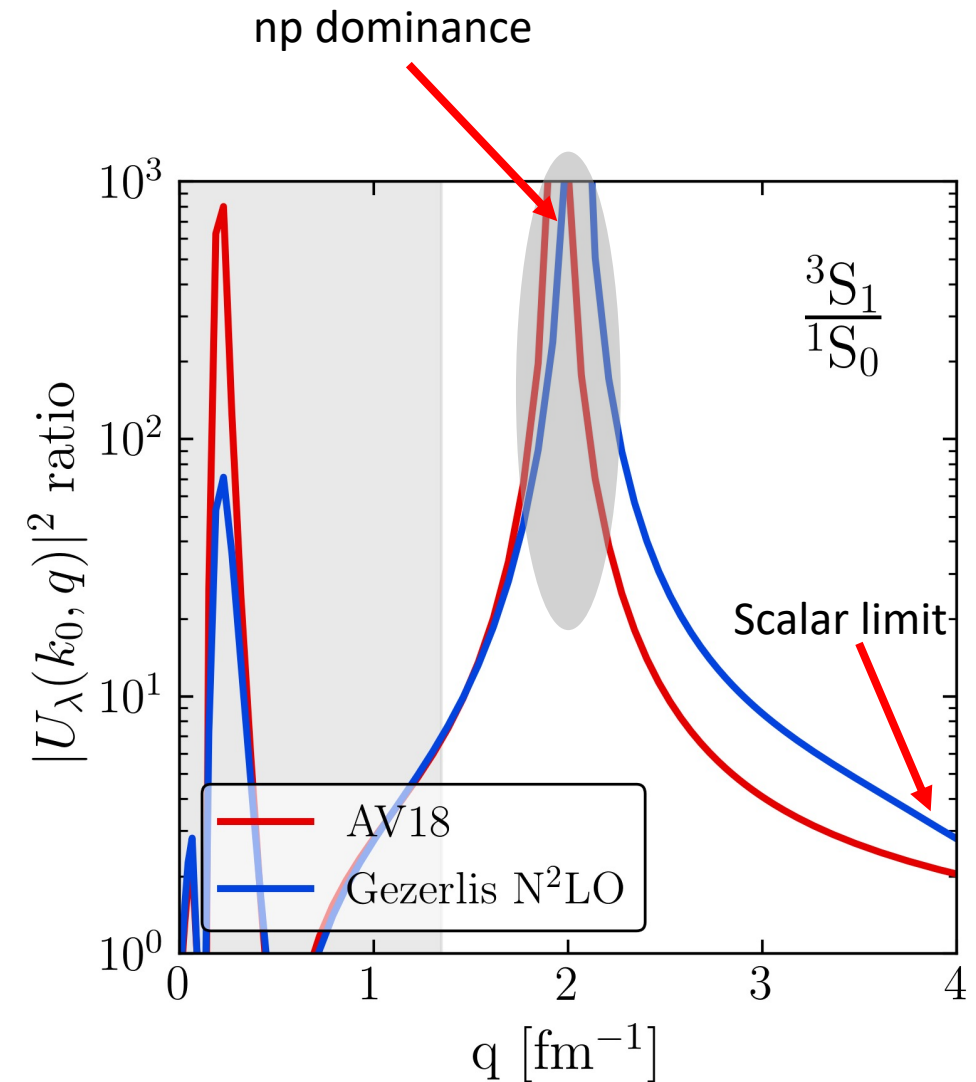
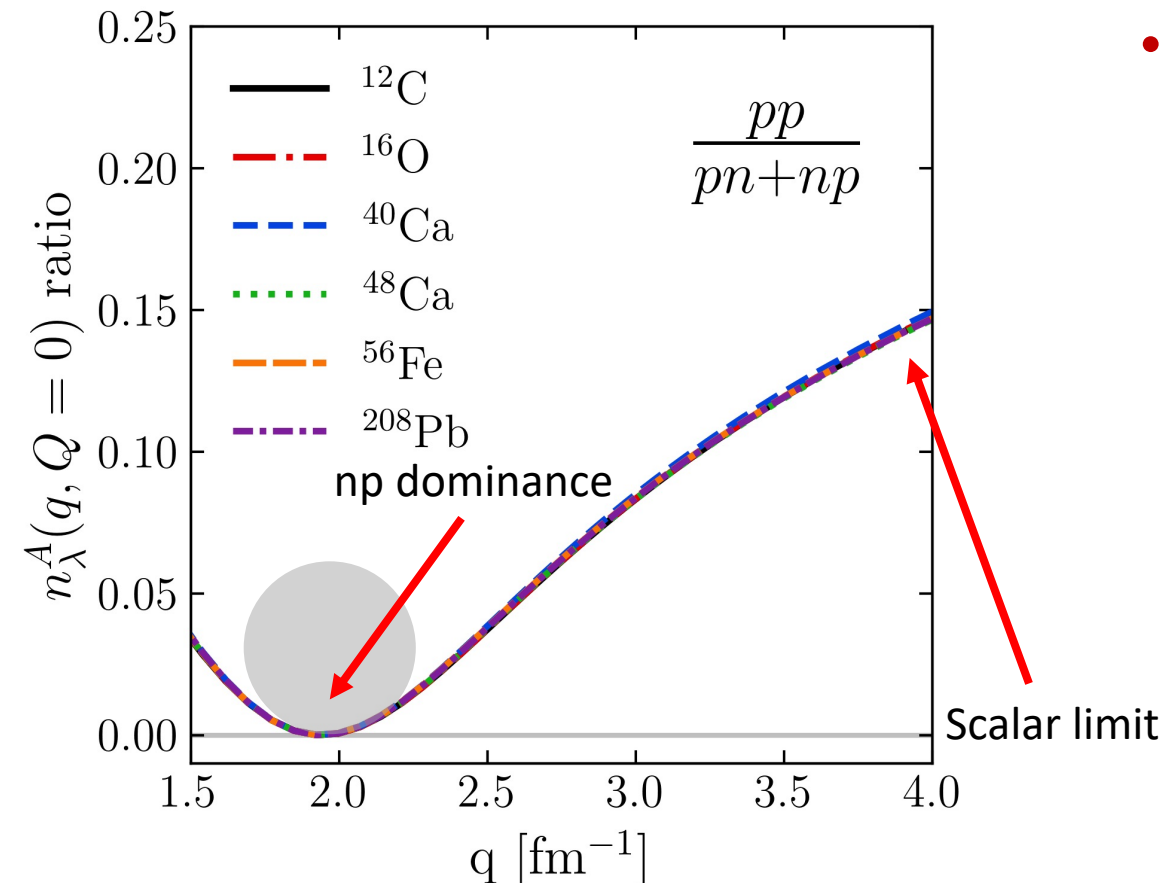


**Fig. 9:**  $^3S_1$  to  $^1S_0$  ratio of SRG-evolved momentum projection operators  $a_q^\dagger a_q$  where  $\lambda = 1.35 \text{ fm}^{-1}$ .

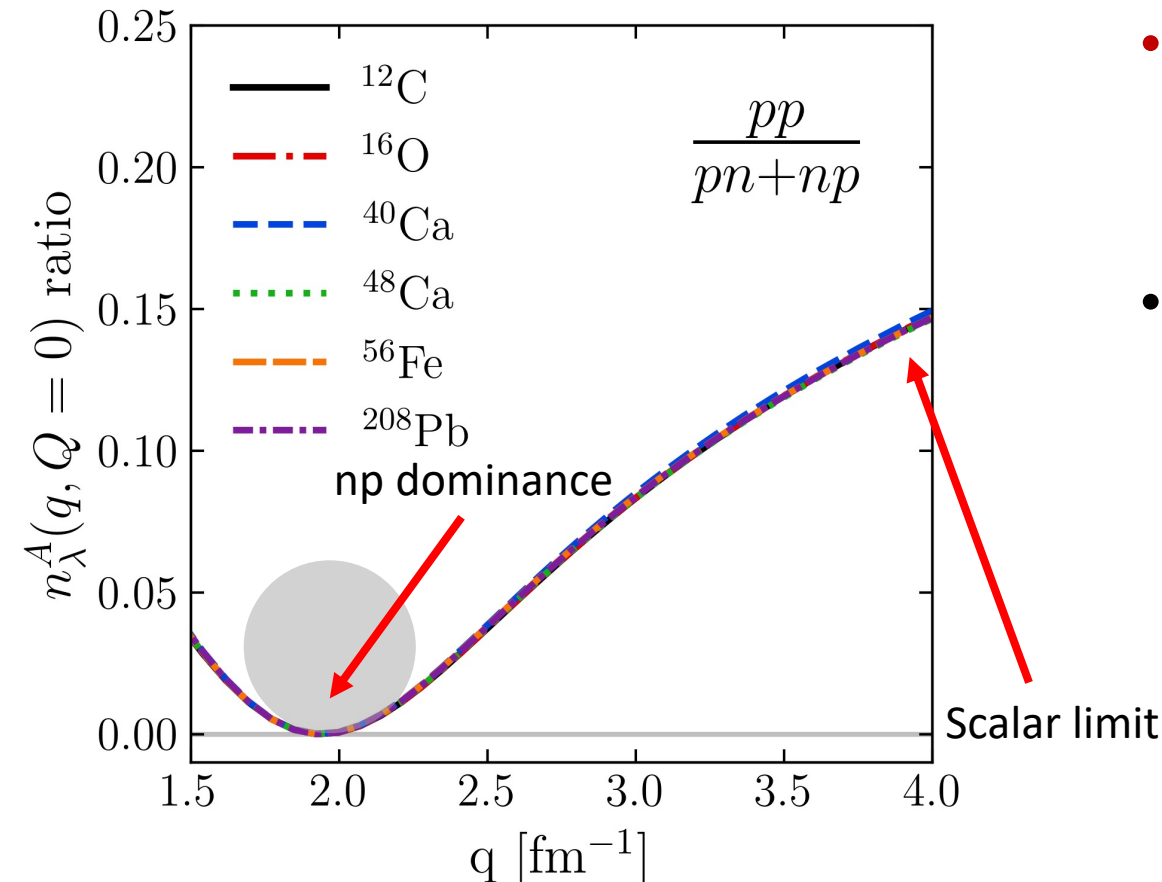
# SRC phenomenology



- Low RG resolution picture reproduces the characteristics of cross section ratios using simple approximations

**Fig. 10:** pp/pn ratio of pair momentum distributions under HF+LDA with AV18 and  $\lambda = 1.35$  fm $^{-1}$ .

# SRC phenomenology

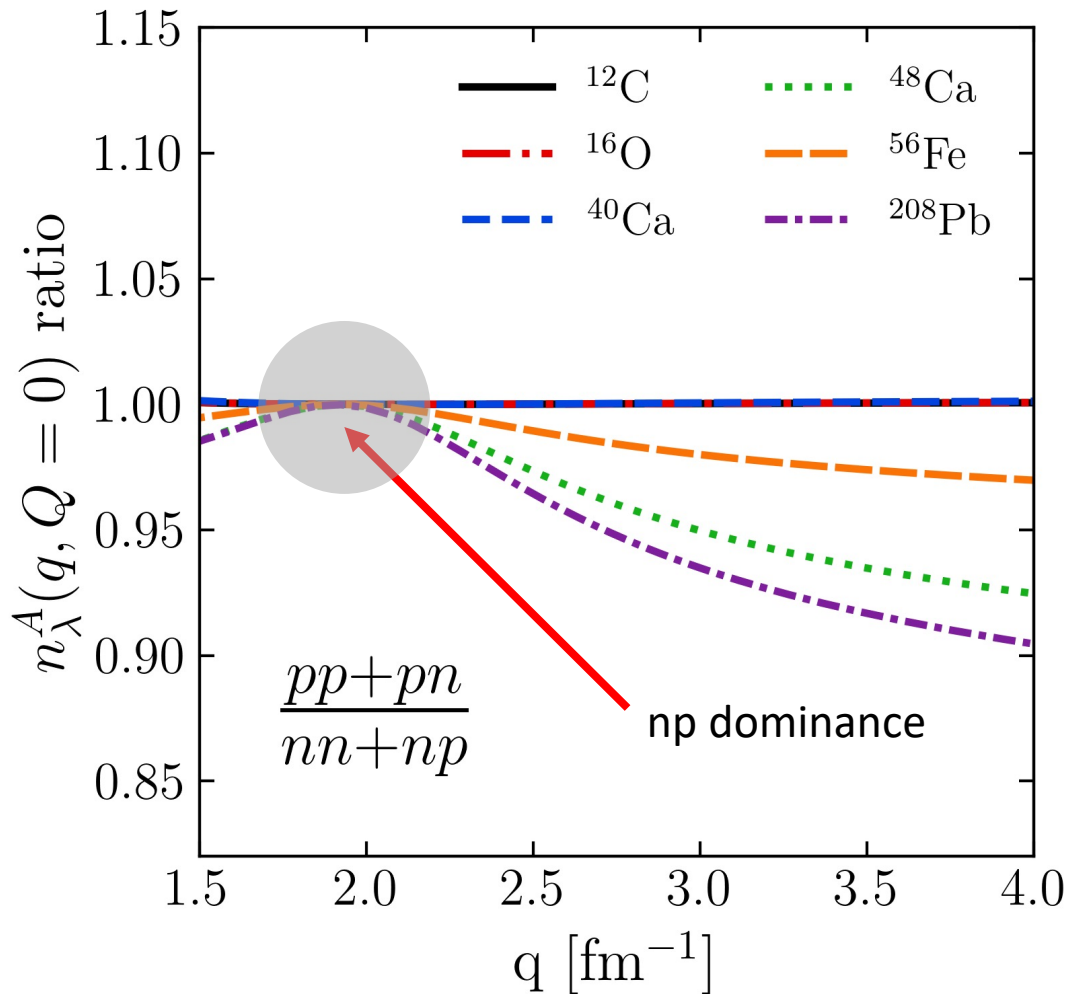


- Low RG resolution picture reproduces the characteristics of cross section ratios using simple approximations
- Weak nucleus dependence from factorization

$$\text{Ratio} \approx \frac{|F_{pp}^{hi}(\mathbf{q})|^2}{|F_{np}^{hi}(\mathbf{q})|^2} \times \frac{\left\langle \Psi_\lambda^A \left| \sum_{\mathbf{k}, \mathbf{k}'}^\lambda a_{\frac{\mathbf{Q}}{2} + \mathbf{k}}^\dagger a_{\frac{\mathbf{Q}}{2} - \mathbf{k}}^\dagger a_{\frac{\mathbf{Q}}{2} - \mathbf{k}'}^\dagger a_{\frac{\mathbf{Q}}{2} + \mathbf{k}'}^\dagger \right| \Psi_\lambda^A \right\rangle}{\left\langle \Psi_\lambda^A \left| \sum_{\mathbf{k}, \mathbf{k}'}^\lambda a_{\frac{\mathbf{Q}}{2} + \mathbf{k}}^\dagger a_{\frac{\mathbf{Q}}{2} - \mathbf{k}}^\dagger a_{\frac{\mathbf{Q}}{2} - \mathbf{k}'}^\dagger a_{\frac{\mathbf{Q}}{2} + \mathbf{k}'}^\dagger \right| \Psi_\lambda^A \right\rangle}$$

**Fig. 10:** pp/pn ratio of pair momentum distributions under HF+LDA with AV18 and  $\lambda = 1.35$   $\text{fm}^{-1}$ .

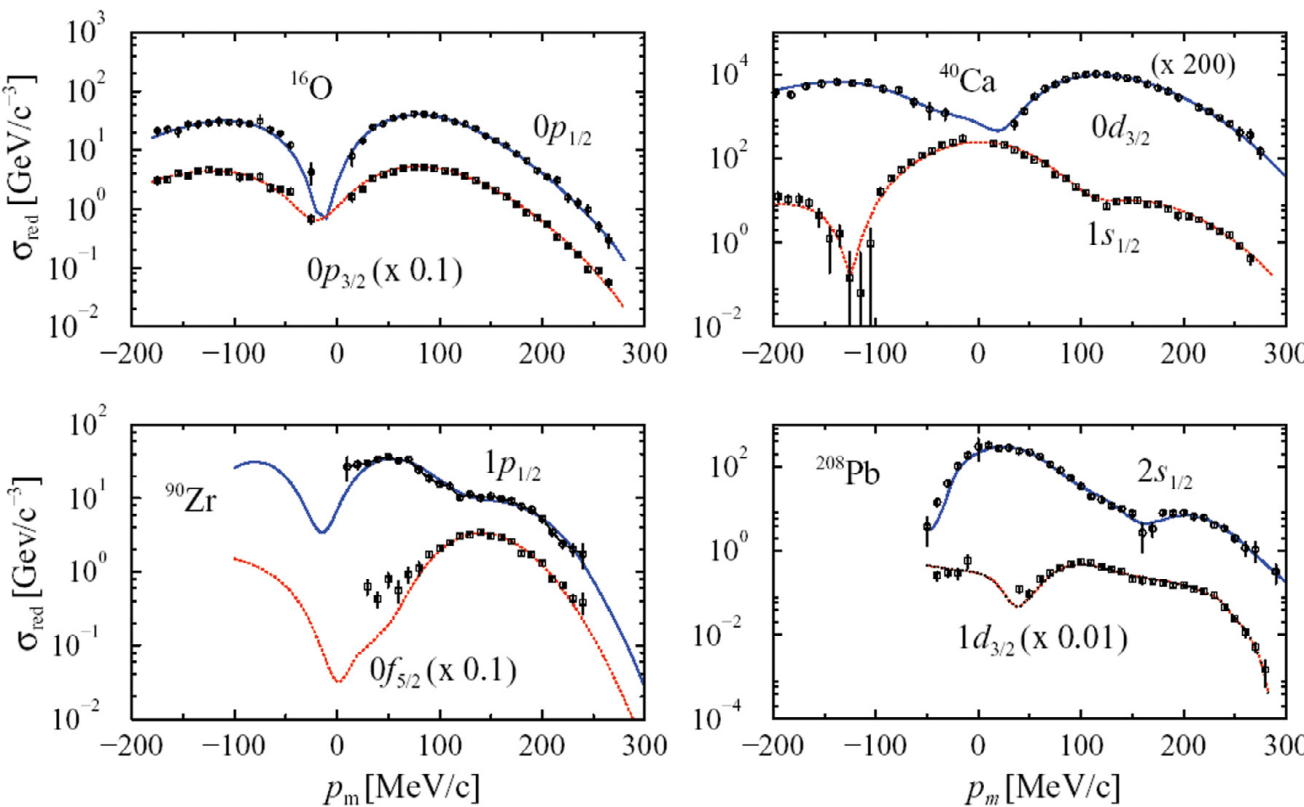
# SRC phenomenology



- Ratio  $\sim 1$  independent of N/Z in np dominant region
- Ratio  $< 1$  for nuclei where  $N > Z$  and outside np dominant region

**Fig. 11:**  $(\text{pp}+\text{pn})/(\text{nn}+\text{np})$  ratio of pair momentum distributions under HF+LDA with AV18 and  $\lambda = 1.35 \text{ fm}^{-1}$ .

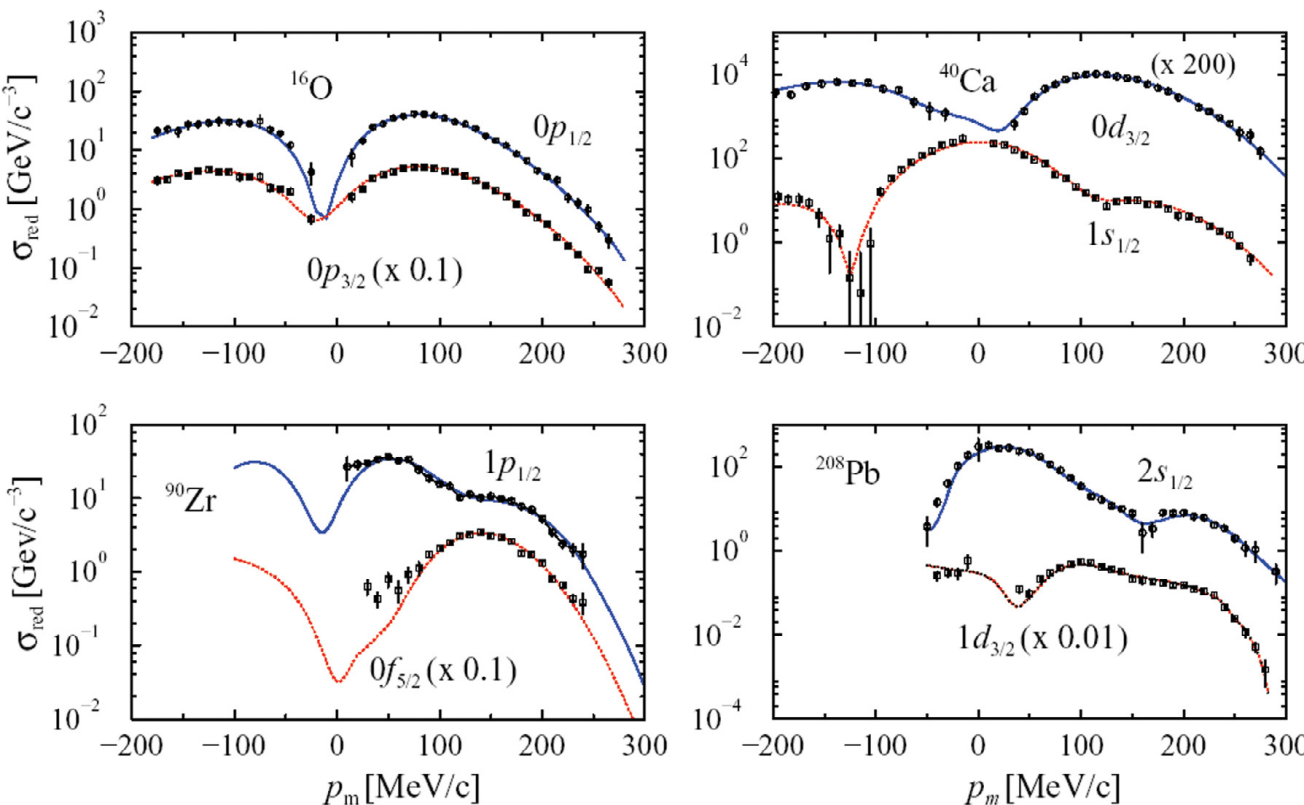
# Other exclusive knockout reactions



- Apply similar low RG analysis to exclusive knockout reactions in  $(e,e'p)$  scattering
- Nucleon knocked out from specific shell model state of target nucleus  $A$

**Fig. 12:** Momentum profiles as function of missing momentum for valence holes in nuclei. Data (black points) from NIKHEF experiments. Figure from T. Aumann et al., Prog. Part. Nucl. Phys. **118**, 103847 (2021).

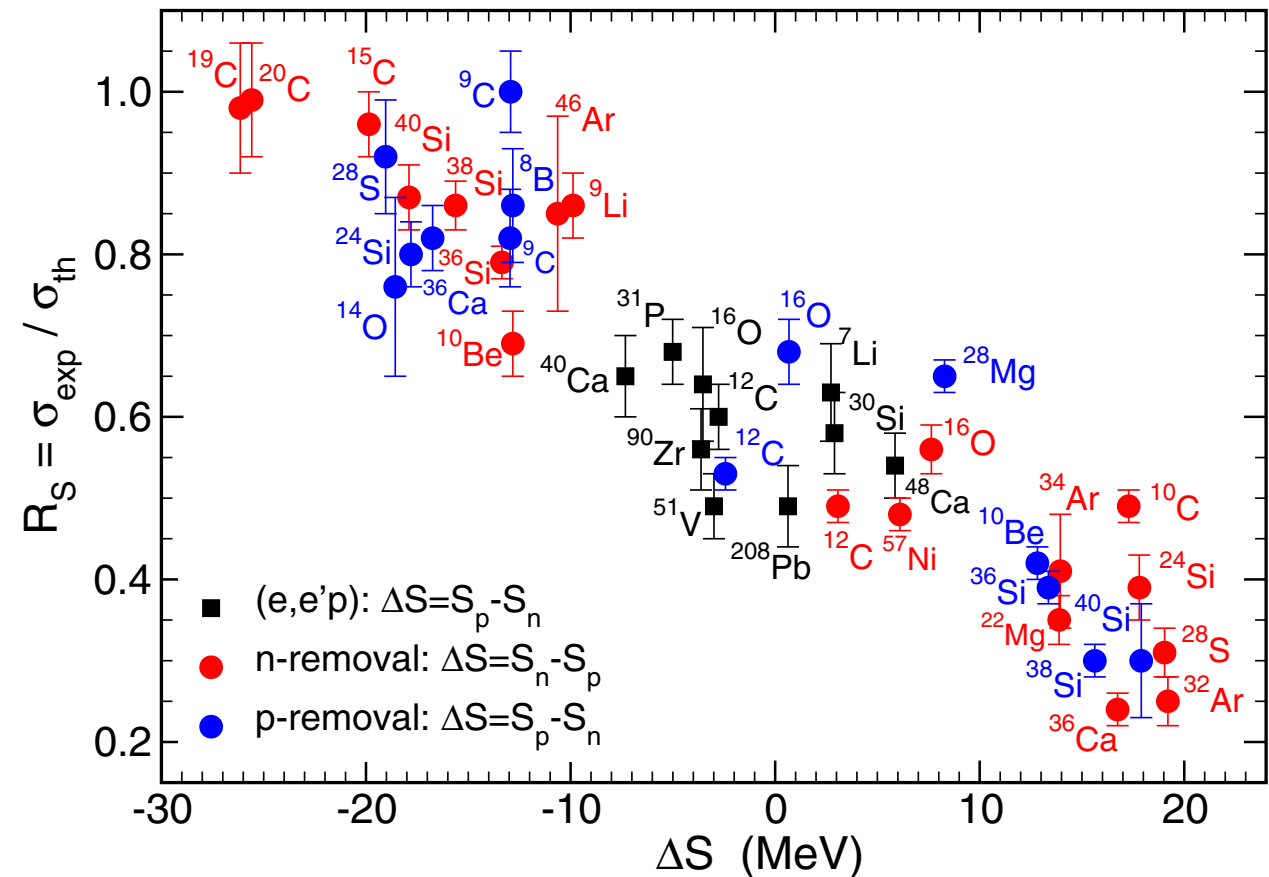
# Other exclusive knockout reactions



- Apply similar low RG analysis to exclusive knockout reactions in  $(e,e'p)$  scattering
- Nucleon knocked out from specific shell model state of target nucleus  $A$
- Momentum dependence of  $(e,e'p)$  exclusive cross section is dominated by the single-particle (sp) wave function
- Spectroscopic factor needed to reduce the theoretical cross section to match experiment

**Fig. 12:** Momentum profiles as function of missing momentum for valence holes in nuclei. Data (black points) from NIKHEF experiments. Figure from T. Aumann et al., Prog. Part. Nucl. Phys. **118**, 103847 (2021).

# Other exclusive knockout reactions



- Systematic trend for discrepancy in exp/theory as a function of  $\Delta S$
- RG analysis can help understand the cause of  $R = \frac{\sigma_{\text{exp}}}{\sigma_{\text{theory}}} < 1$
- Mismatch of scale between one-body (**high RG**) operator and shell model structure (**low RG**) gives  $\sigma_{\text{theory}} > \sigma_{\text{exp}}$

**Fig. 13:**  $R$  as a function of  $\Delta S$ . Red (blue) points correspond to neutron-removal (proton-removal) cases. Solid black squares correspond to electron-induced proton knockout data. Figure from J. A. Tostevin and A. Gade, Phys. Rev. C **90**, 057602 (2014).

# Other exclusive knockout reactions

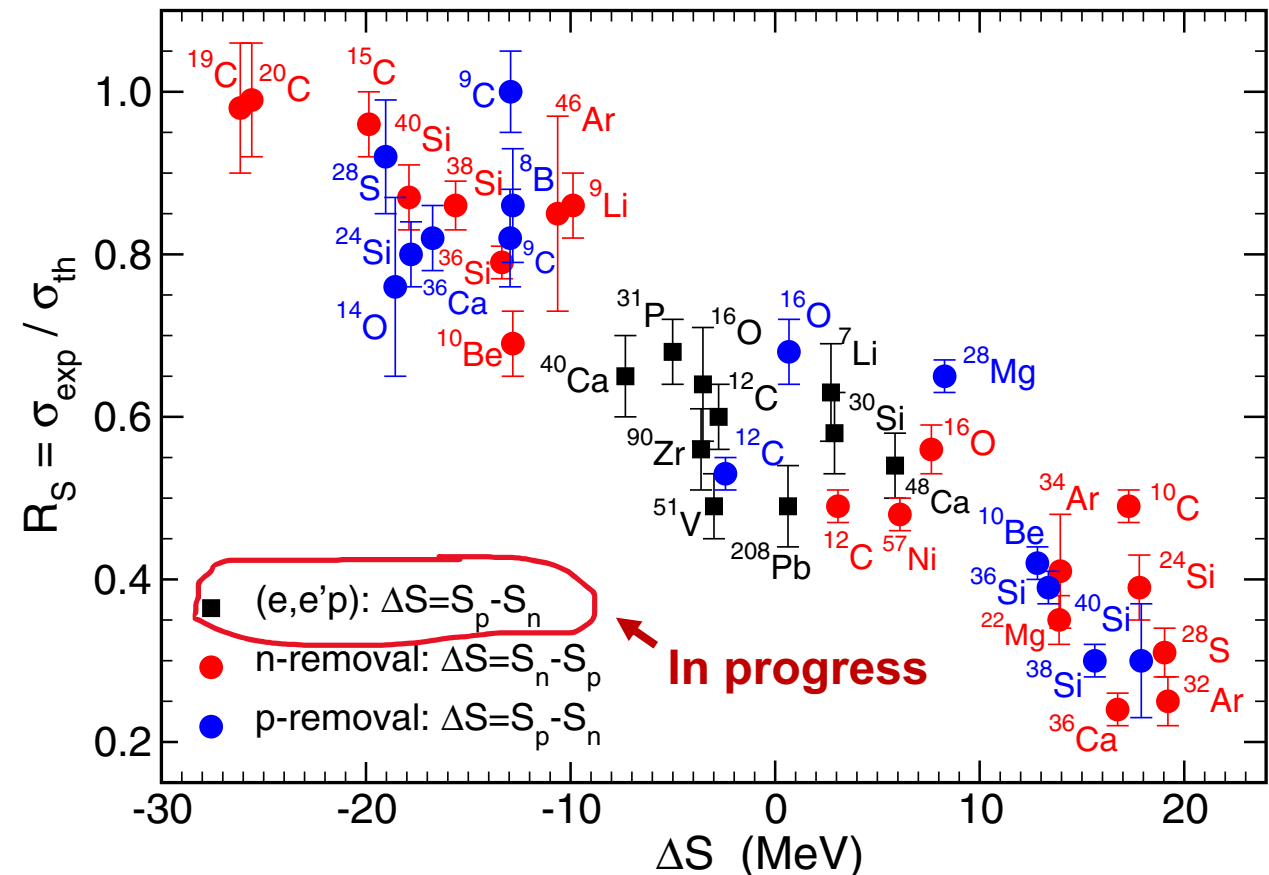


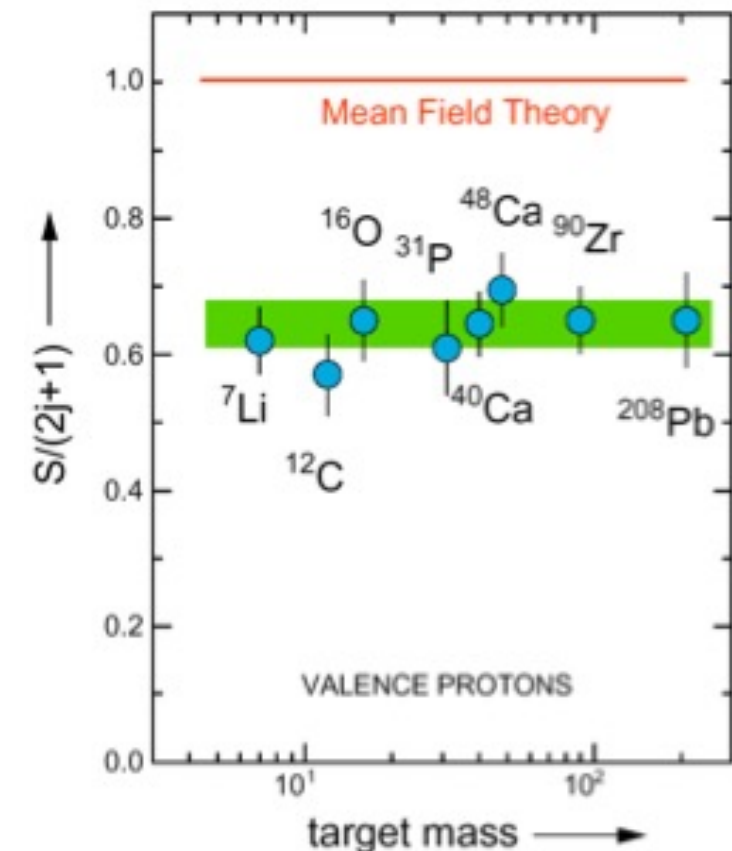
Fig. 13:  $R$  as a function of  $\Delta S$ . Red (blue) points correspond to neutron-removal (proton-removal) cases. Solid black squares correspond to electron-induced proton knockout data. Figure from J. A. Tostevin and A. Gade, Phys. Rev. C **90**, 057602 (2014).

- Systematic trend for discrepancy in exp/theory as a function of  $\Delta S$
- RG analysis can help understand the cause of  $R = \frac{\sigma_{\text{exp}}}{\sigma_{\text{theory}}} < 1$
- Mismatch of scale between one-body (**high RG**) operator and shell model structure (**low RG**) gives  $\sigma_{\text{theory}} > \sigma_{\text{exp}}$
- Currently working on SRG-evolving spectroscopic factors for  $(e, e'p)$  reactions
- Note, spectroscopic factors are scale/scheme dependent

# Spectroscopic factors

- Spectroscopic factor for sp state  $\alpha$  defined in terms of removal amplitude

$$S = \int d\mathbf{p} |\langle \Psi_{\alpha}^{A-1} | a_{\mathbf{p}} | \Psi_0^A \rangle|^2$$

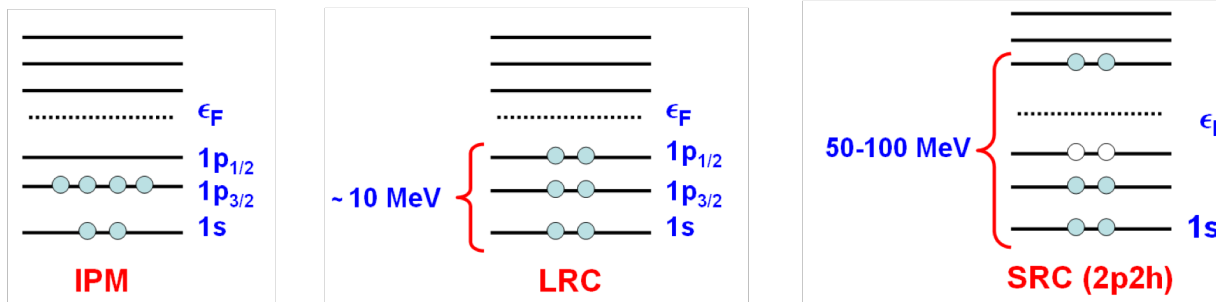


# Spectroscopic factors

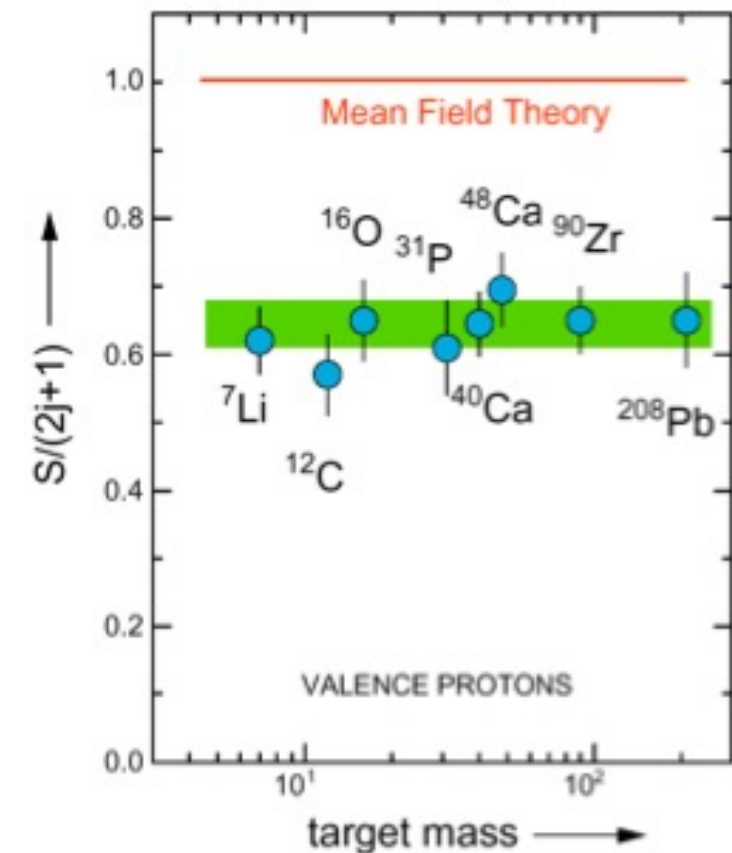
- Spectroscopic factor for sp state  $\alpha$  defined in terms of removal amplitude

$$S = \int d\mathbf{p} |\langle \Psi_{\alpha}^{A-1} | a_{\mathbf{p}} | \Psi_0^A \rangle|^2$$

- sp strength is reduced relative to the independent-particle model (IPM) by correlations: **Long-range correlations (LRC)** and **SRC**



Long-range vs. short-range correlations



# Spectroscopic factors

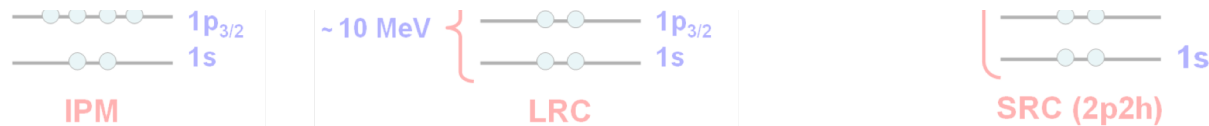
- Spectroscopic factor for sp state  $\alpha$  defined in terms of removal amplitude

$$S = \int d\mathbf{p} |\langle \Psi_{\alpha}^{A-1} | a_{\mathbf{p}} | \Psi_0^A \rangle|^2$$

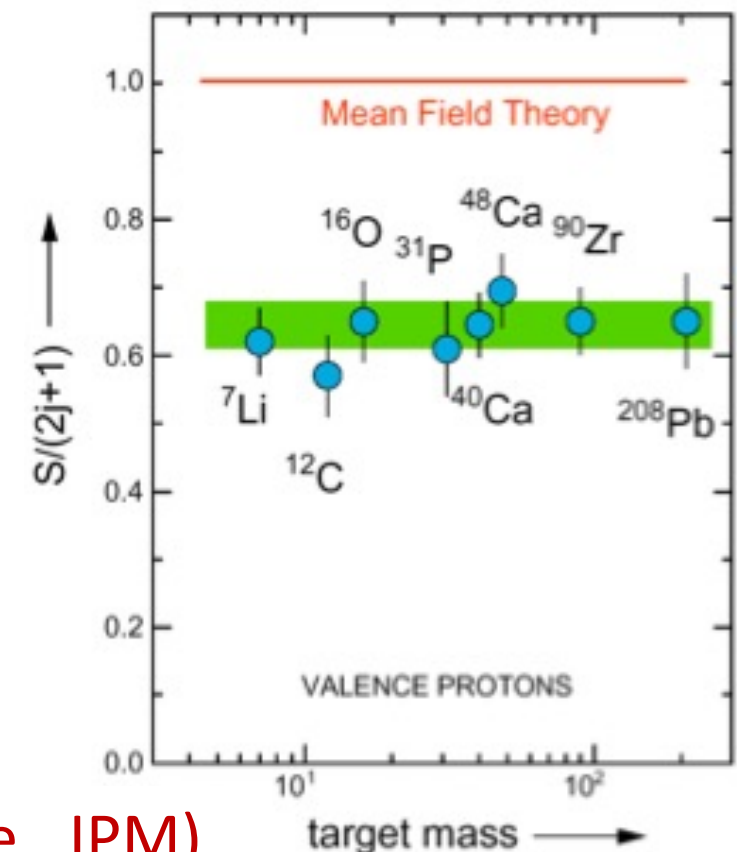
- sp strength is reduced relative to the independent-particle model (IPM) by correlations: **Long-range correlations (LRC)** and **SRC**



**Idea:** SRG evolve and analyze using simple approximations (i.e., IPM)



Long-range vs. short-range correlations



# Summary

- At low renormalization group (RG) resolution, simple approximations to SRC physics work and are systematically improvable
- Results suggest that we can analyze high-energy nuclear reactions using low RG resolution structure (e.g., shell model) and consistently evolved operators
  - Matching resolution scale between structure and reactions is crucial!

# Summary

- At low renormalization group (RG) resolution, simple approximations to SRC physics work and are systematically improvable
- Results suggest that we can analyze high-energy nuclear reactions using low RG resolution structure (e.g., shell model) and consistently evolved operators
  - Matching resolution scale between structure and reactions is crucial!
- **Outlook:**
  - Extend to  $(e, e' p)$  knockout cross sections and test scale/scheme dependence of extracted properties
  - Investigate impact of various corrections (e.g., 3-body terms)
  - Apply to more complicated knockout reactions (SRG with optical potentials)
  - Implement uncertainty quantification in low RG resolution calculations

# Extras

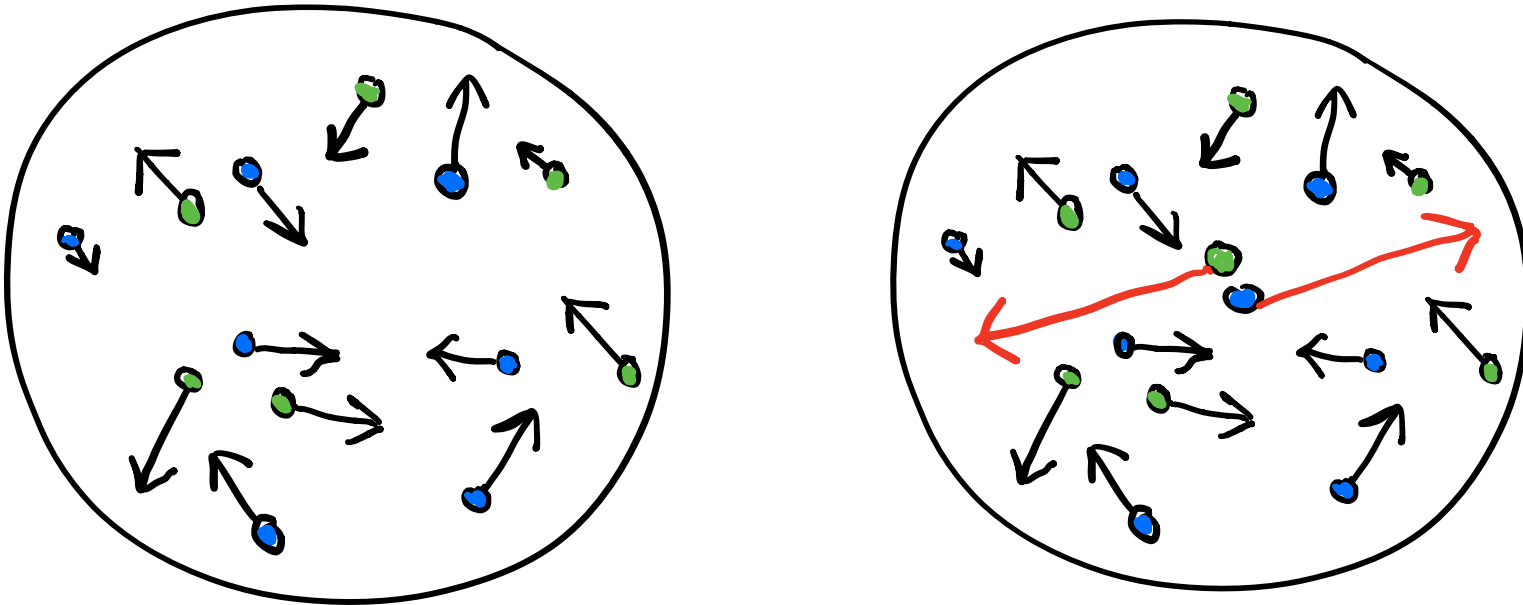
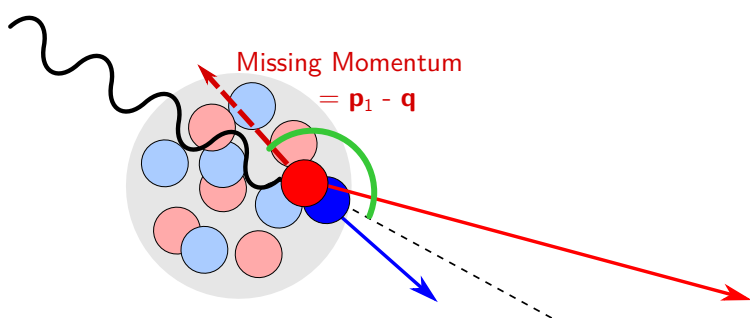
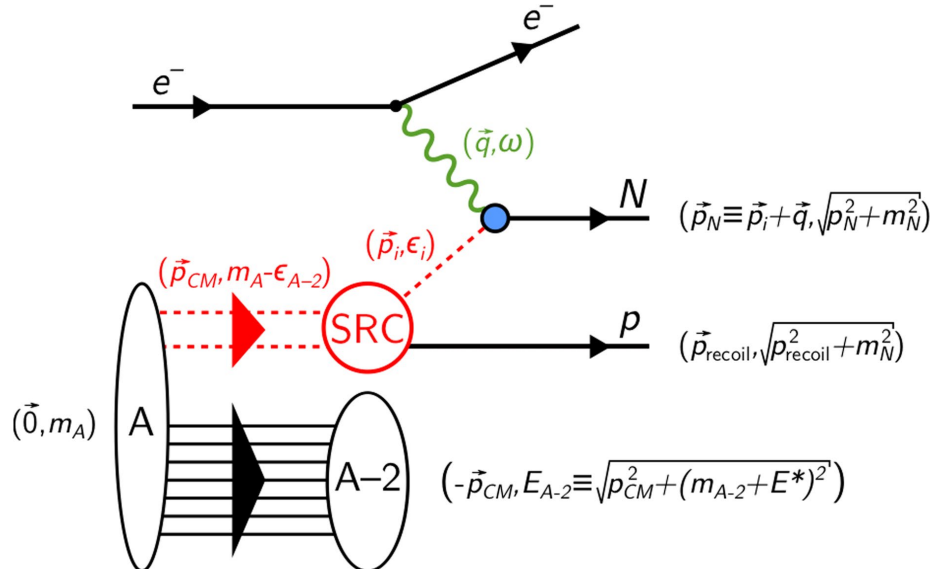


**Fig. 14:** Cartoon snapshots of a nucleus at (left) low-RG and (right) high-RG resolutions. The back-to-back nucleons at high-RG resolution are an SRC pair with small center-of-mass momentum.

# Extras



- Kinematics chosen such that two-nucleon knock-out dominates
- Break up the pair, detect both nucleons, and reconstruct initial state
- Kinematics minimize final state interactions and meson exchange currents

# Extras

**Universality:** Low-energy physics of different interactions becomes the same at low RG resolution

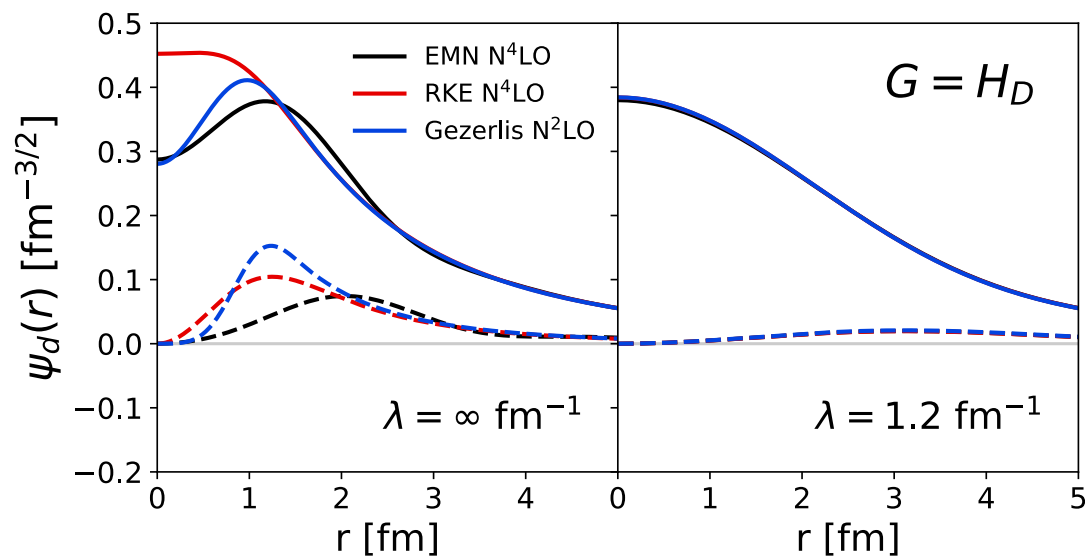


**Fig. 15:** Initial and SRG-evolved deuteron wave functions in coordinate space for several chiral interactions.

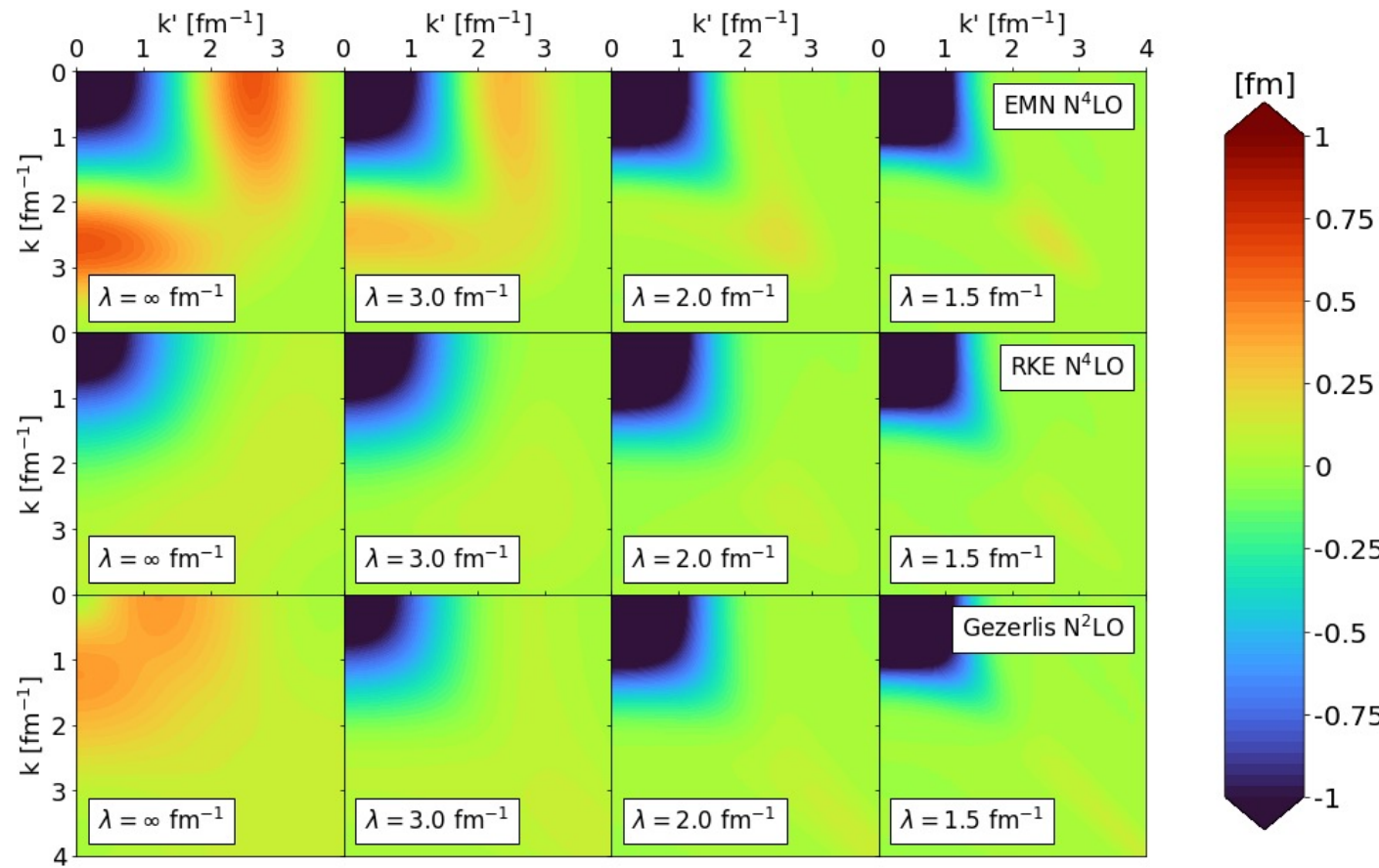
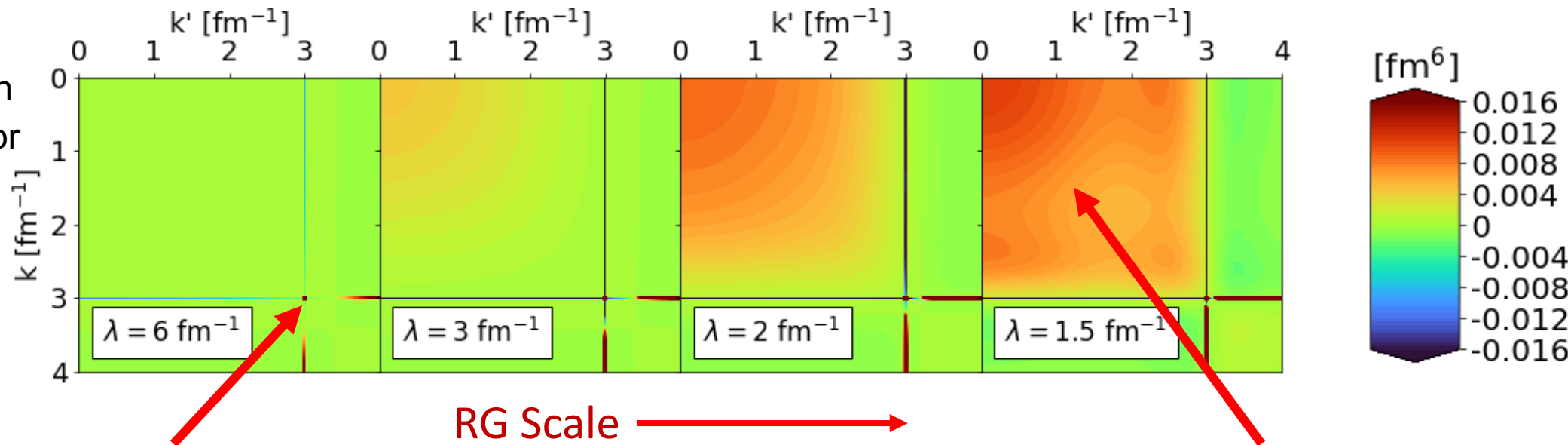


**Fig. 16:** SRG evolution for several chiral interactions in the  $^3S_1 - ^3S_1$  channel.

# Extras

**Fig. 17:** Evolved momentum projection operator  $U_\lambda a_q^\dagger a_q U_\lambda^\dagger$  for several  $\lambda$  values where  $q = 3 \text{ fm}^{-1}$ .



Initial operator is a discretized delta function in momentum space  
 $\sim \delta(k - q)\delta(k' - q)$

SRG evolution induces smooth, low-momentum contributions

# Extras

**Fig. 17:** Evolved momentum projection operator  $U_\lambda a_q^\dagger a_q U_\lambda^\dagger$  for several  $\lambda$  values where  $q = 3 \text{ fm}^{-1}$ .

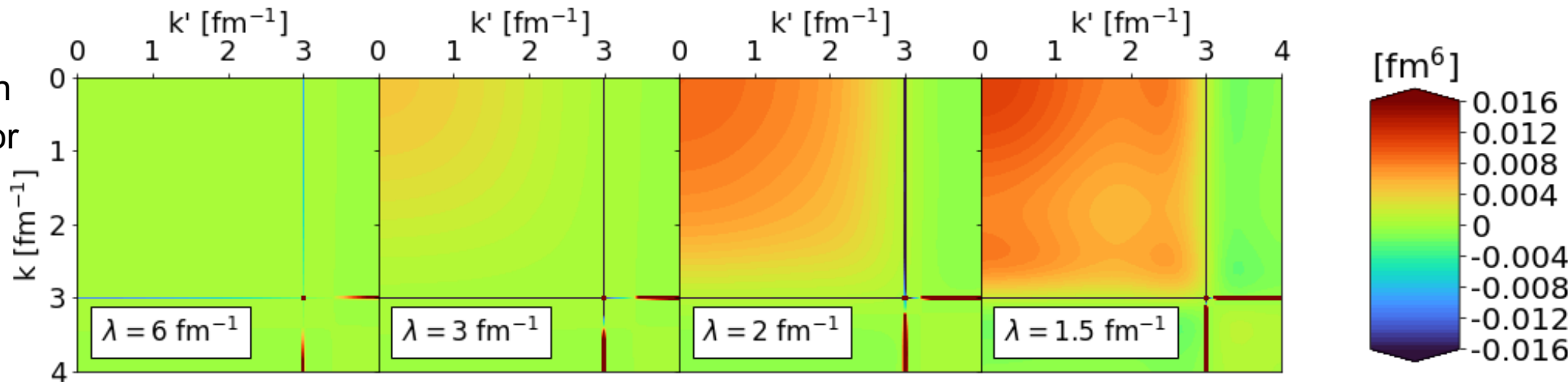
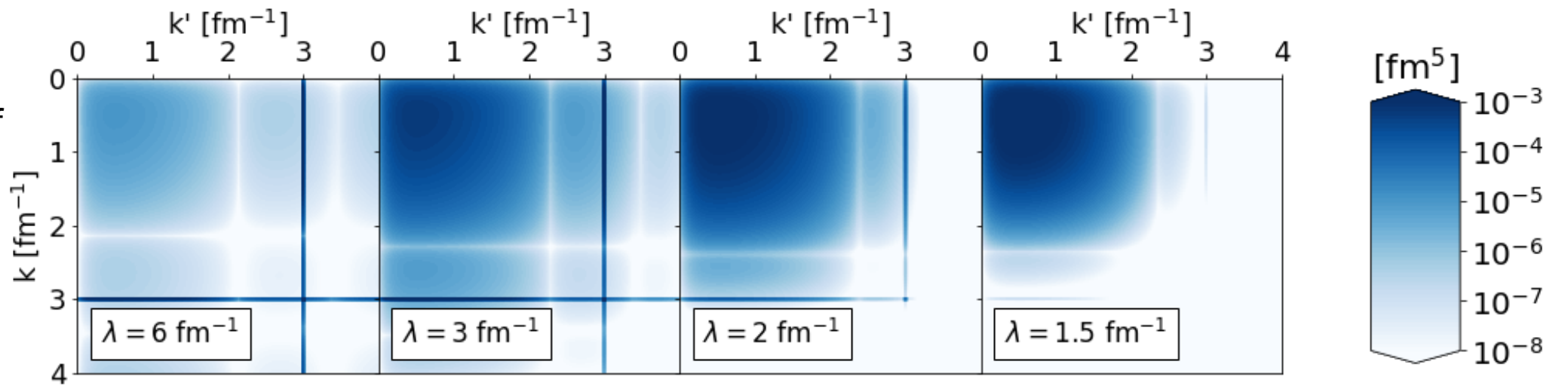


**Fig. 18:** Integrand of  $\langle \psi_d^\lambda | U_\lambda a_q^\dagger a_q U_\lambda^\dagger | \psi_d^\lambda \rangle$  where  $q = 3 \text{ fm}^{-1}$ .



# Extras

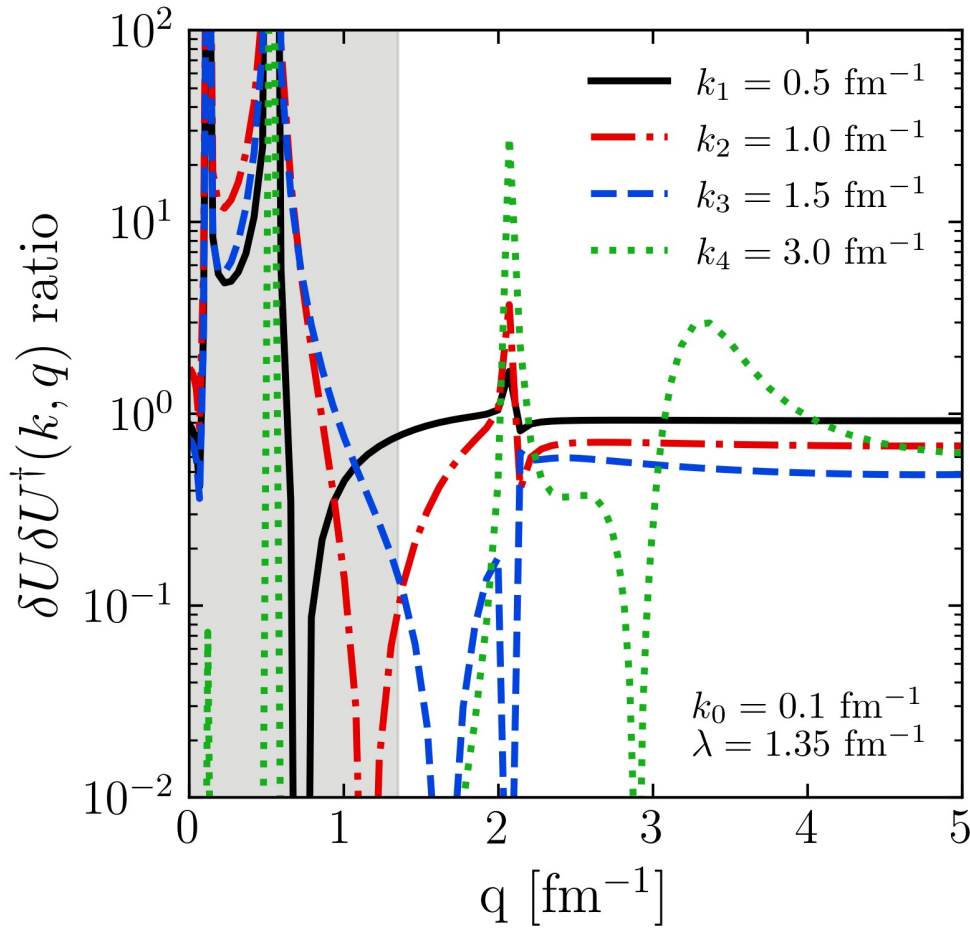


**Fig. 19:** Ratio of  $\delta U \delta U^\dagger(k, q)$  for fixed  $k$  and  $\lambda$ .

- Consider an operator dominated by high momentum  $q$  where  $k < \lambda$  and  $q \gg \lambda$
- Expand the eigenstates  $\psi_\alpha^\infty$  of the initial NN Hamiltonian in terms of the SRG-evolved states  $\psi_\alpha^\lambda$

$$\psi_\alpha^\infty(q) \approx \gamma^\lambda(q) \int_0^\lambda d\tilde{p} Z(\lambda) \psi_\alpha^\lambda(p) + \eta^\lambda(q) \int_0^\lambda d\tilde{p} p^2 Z(\lambda) \psi_\alpha^\lambda(p) + \dots$$

- Substitute leading-order term of operator product expansion (OPE) in spectral representation of SRG transformation

$$\begin{aligned} U_\lambda(k, q) &= \sum_{\alpha}^{\infty} \langle k | \psi_\alpha^\lambda \rangle \langle \psi_\alpha^\infty | q \rangle \\ &\stackrel{|E_\alpha| \ll |E_{QHQ}|}{\approx} \left[ \sum_{\alpha} \langle k | \psi_\alpha^\lambda \rangle \int_0^\lambda d\tilde{p} Z(\lambda) \psi_\alpha^{\lambda\dagger}(p) \right] \gamma^\lambda(q) \\ &\equiv K_\lambda(k) Q_\lambda(q) \end{aligned}$$